Towards cardiovascular stents fabricated by stereolithography

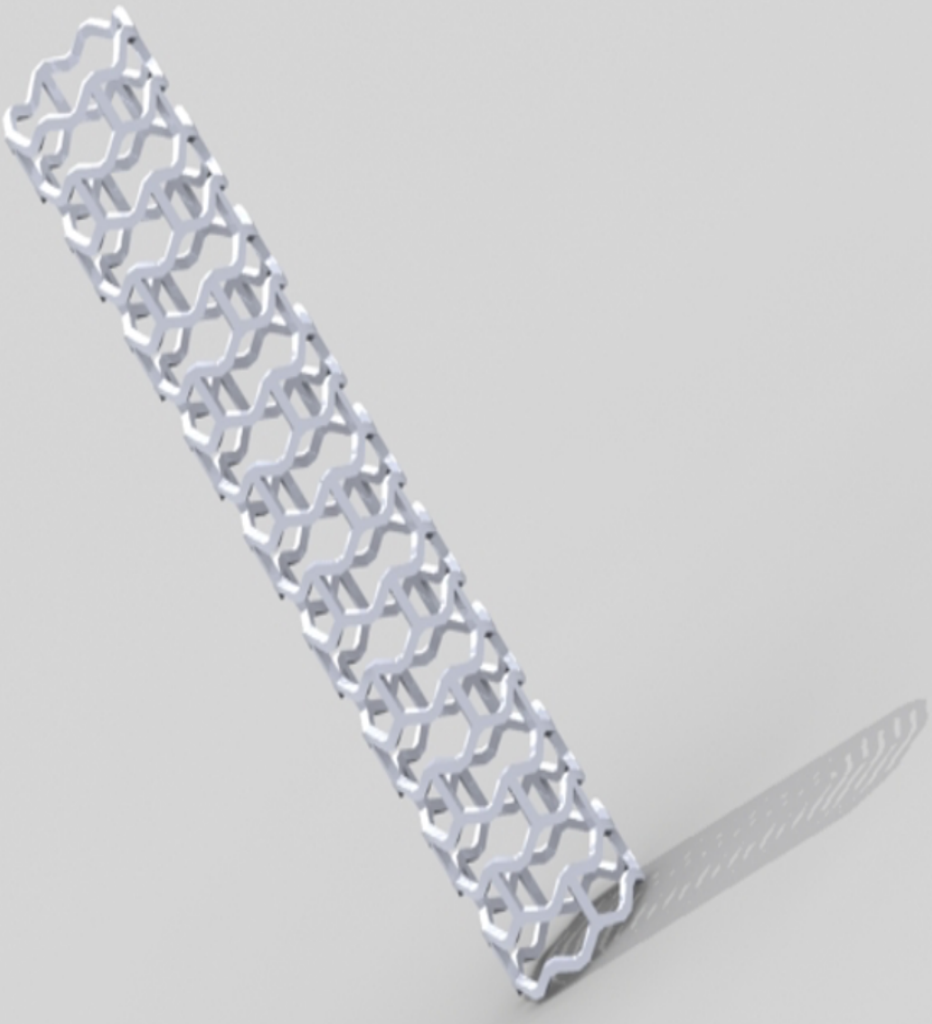

TU Delft

Thomas van den Brekel
MSc Biomedical Engineering

Towards cardiovascular stents fabricated by stereolithography

Master Thesis

by

Thomas van den Brekel

to obtain the degree of

Master of Science
in Biomedical Engineering

at the Delft University of Technology,
to be defended publicly on Tuesday May 18, 2021 at 10:30 AM.

Student number:	4395417	
Project duration:	June 1, 2020 – May 18, 2021	
Supervisors:	Dr. ir. I. Apachitei,	TU Delft, supervisor
	Dr. M. Leemhuis,	The Hague University of Applied Sciences
Thesis committee:	Prof. dr. ir. A. Zadpoor,	TU Delft
	Dr. ir. I. Apachitei,	TU Delft, supervisor
	Dr. M. Leemhuis,	The Hague University of Applied Sciences
	Dr. J.J. van den Dobbelsteen,	TU Delft

This thesis is confidential and cannot be made public until Januari 31, 2022.

TU Delft

Preface

Cardiovascular diseases are the leading cause of death worldwide. Atherosclerosis, responsible for 80% of cardiovascular deaths, is nowadays treated with stents, which scaffold the balloon-dilated artery and seals the dissection flaps. The importance of cardiovascular stents in positively contributing to global health, supports research and development for new affordable manufacturing techniques. To improve the quality of treatment, decrease chronic inflammation and enhance vascular healing, the focus on future stent design moved to the development of bioresorbable stents. Additive Manufacturing, or so-called 3D printing, methods generate the opportunity to respond to the increasing request for patient-specific medical implants.

This thesis describes the project that was conducted with the aim of developing an additive manufactured bioresorbable polymeric cardiovascular stent. With the ultimate goal to fabricate on-the-spot and on-demand patient specific drug-eluting bioresorbable stents. This study disclosed the obstacles and minimal standards on capabilities, features and dimensions for the development of next generation bioresorbable stents manufactured on site.

This thesis would not have been possible without the help of numerous people. Predominately, I would like to thank both my supervisors Dr. Mark Leemhuis and Dr. Ir. Iulian Apachitei for being excellent mentors and their continuous advice and guidance. Both your knowledge and experience in 3D printing, biomaterials and science in general fed my interest and motivated me to strive for the best possible outcome. The long meetings we spent discussing all forthcoming obstacles, accomplishments and subsequent steps, but also the quick panic conversations or calls are very much appreciated. I sincerely value your continuous availability, support and believe in my abilities to pursue this ambitious graduation project.

I would also like to thank Prof. Dr. Ir. Amir Zadpoor for taking time to take part in my evaluation committee.

Also, I would like to thank Katerina Isaakidou, Sander Leeflang and Niko Putra from the Biomaterials & Tissue Biomechanics group at the TU Delft, Rugene Leito from the Hague University of Applied Sciences and Christiaan Horsman who supported me in one way or another with feedback, equipment and interesting conversations.

Last but not least, I would like to thank my family and friends for their continuous support. Hopefully, with this research I can make a small contribution to the -above mentioned- overall goal.

Thomas van den Brekel
Delft, May 2021

Acronyms

3D	Three-dimensional
AM	Additive Manufacturing
AFM	Atomic Force Microscopy
BMS	Bare metal stent
BPM	Beats per minute
B-ink	Biomaterial ink
BRS	Bioresorbable stent
CAD	Coronary artery disease
CAD-file	computer aided design file
CoCr	Cobalt-Chromium
DES	Drug Eluting Stent
FDA	Food and Drug Administration
HV	High Vacuum
IPA	2-propanol
LED	Light-emitting diode
LT	layer thickness
Mw	molecular weight
NMR	Nuclear Magnetic Resonance
OD	outer diameter
PCL	Poly(ϵ -caprolactone)
PCI	Percutaneous coronary intervention
PGA	Polyglycolic acid
PLA	Polylactide acid
PtCr	Platinum chromium
PU	Polyurethanes
RT	Room temperature
SED	Secondary Electron Detector
SLA	Steriolithography
SS	316L Stainless steel
Tg	Transition temperature
UV	Ultra Violet

Glossary

Endothelialization The process of lining the microchannel lumen with a monolayer of endothelial cells

Neointimal proliferation The proliferation and migration of vascular smooth muscle cells

Late lumen loss The angiographic minimum lumen diameter immediately after percutaneous transluminal angioplasty minus the minimum lumen diameter at angiographic follow-up

Stenosis An abnormal narrowing in a blood vessel, leading to restricted bloodflow

Restenosis The recurrence of stenosis

In-stent restenosis The incident of restenosis when a stent is deployed

Thrombosis The formation of a blood clod in a blood vessel

Tunica intima The innermost layer of a blood vessel

Target lesion vascularization Vascularization of the vessel wall in the proximity of the implanted stent

Vasomotion Spontaneous rhythmical contraction–relaxation mechanism of blood vessel walls

Contents

Abstract

Currently, cardiovascular diseases are the leading cause of death worldwide, and a global ageing population ensures increasing numbers for the foreseeable future. Atherosclerosis, responsible for 80% of cardiovascular deaths, is nowadays treated with stents, which scaffold the balloon-dilated artery and seals the dissection flaps. In 2016, the Absorb GT1 (Abbott, USA) was approved by the FDA as the first bioresorbable stent (BRS), which further stimulated the research on degradable polymeric biomaterials. Polymeric BRS showed comparable characteristics as the most often used, drug-eluting stents (DES), with the added advantage of being fully biodegradable within two years. However, as several hurdles still need to be tackled, research to obtain the perfect BRS continues. A limited range of geometries and sizes influences the adaptation of the scaffold in a patient's vessel, which subsequently affects the therapeutic outcome. Additive manufacturing (AM) could potentially be a method to produce cost-effective and patient-specific cardiovascular stents. This study aimed to contribute to innovations leading to the development of a next-generation stent. It presents novel information on Stereolithography (SLA) usability for the 3D printing of BRS and highlights the effects of structural and mechanical limitations, which are all inherent to the materials selection. Development and progress on specific capabilities have revealed and emphasized shortcomings in other domains. Fine-tuning the SLA printer settings and limitations, we were able to 3D print a 3 mm stent with promising morphological and mechanical characteristics. Future research and development should encompass all aspects of stent application, from manufacturing to deliverability, from functionality to solvability.

1 Introduction

1.1. Atherosclerosis and stenting

Cardiovascular diseases are the leading cause of death worldwide. As the world population grows and its longevity extends, the annual cardiovascular disease mortality numbers are expected to increase substantially from 17.5 million in 2012 to 22.2 million in 2030. The exact cause of cardiovascular diseases is still unclear; however, various risk factors increase the potential chances of developing these diseases, such as hypertension, smoking, high cholesterol, diabetes, inactivity, overweight, family history, age and alcohol[1]. Circa 80% of deaths by cardiovascular diseases are due to atherosclerosis in the arteries of the heart, which causes Coronary artery disease (CAD) (e.g. angina/ heart attacks/ heart failure) and stroke [2]. Atherosclerosis is a disease in which plaque builds up on the inside of the artery wall. As a result, the artery becomes narrower, and the amount of oxygen-rich blood distributed through the body diminishes [3]. Various studies highlighted different types of plaque, depending on their development timeline and their location. The pathophysiologic process by which atherosclerosis occurs is a complex four stage process. First, endothelial cell injury is likely to initiate the atherosclerotic plaque formation due to the constant exposure to the circulation. Subsequently, lipoprotein molecules can gain entry at the disrupted endothelium where they are modified by oxidation or glycation. This modified lipoproein is inflammatory and able to be ingested by macrophages is the arteial wall, attracting an inflammatory reaction. Lastly, smooth muscle cells migrate to the surface of the plaque to create a fibrous cap [4][5][6].

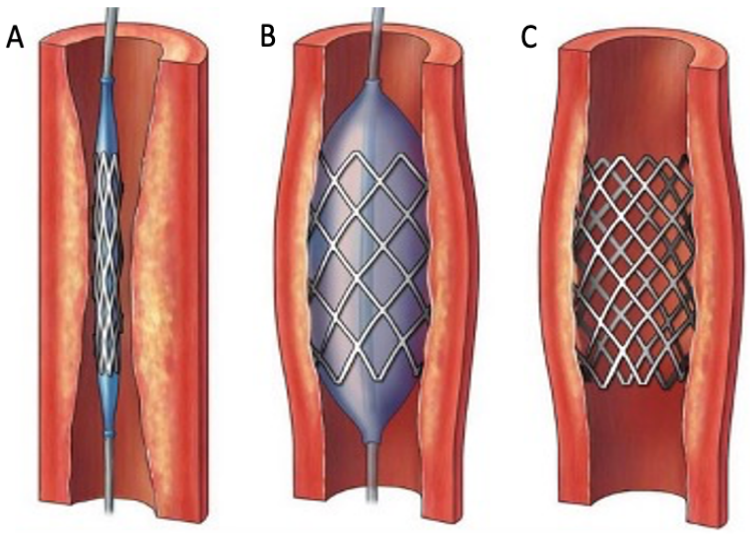

Figure 1.1: The principle of a coronary stent placement; a balloon catheter inserted in a constricted blood vessel (A), volume of balloon increased to help widen the vessel and improve blood flow to your heart (B), placement of a stent to support the balloon-dilated artery [7].

CAD is often treated with Percutaneous coronary intervention (PCI), which generally involves balloon angioplasty and stent implantation. A stent scaffolds the balloon-dilated artery and seals the dissection flaps to reopen obstructed or narrowed arteries (Figure 1.1). Coronary stents contribute to restoring the lumen, stabilising the optimal blood flow of blood vessels, and preventing late recoil. PCI is one of the most common cardiovascular procedures performed in the Western World since its introduction in the 1980s [8][9]. While stenting is considered safe and effective, the remaining problems, such as inflammation, stent thrombosis and in-stent restenosis, are yet to be resolved. A more recent solution is the application of Drug Eluting Stent (DES), to release antiproliferative therapeutics that contribute to the prevention of restenosis. However, unfortunately, complications have not disappeared entirely, and nowadays, myocardial infarction, stent fracture and late in-stent restenosis remain leading DES-related impediments [7]. Consequently, a shift is expected to Bioresorbable stent (BRS).

1.2. Bioresorbable stents

Since the introduction of the first purely metallic stent, multiple aspects have contributed to vascular stent development. The nowadays used DES show short-term benefits such as arterial remodelling, drug release, and mechanical support [10][11]. However, there are still many fundamental off-putting factors like target lesion revascularization, late stent thrombosis, and the device will remain in the body. Last-mentioned is peculiar since clinicians agreed that restenosis is rarely seen later than 12 months after surgery. Arterial patency is commonly recovered within the first six months after the procedure, which corresponds with the potential start of in-stent restenosis. Thus, the clinical need for permanent stent scaffolding is likely to be very limited [7][12][13]. To overcome the disadvantages and limitations of BMS and metallic DES, bioresorbable stents (BRS) have been developed. These devices have gained an increased momentum because they bring the advantages of a non-permanent foreign device in the body and offer short-term mechanical support to the vessel, while lesion healing and arterial remodelling occurs, after which they will resorb into the body. Compared to DES, chronic inflammation is diminished, while vascular healing is improved and restenosis rates are decreased.

The whole bioresorbable stenting process consists of three phases. The first phase is aimed at revascularization. At the end of this phase, complete neointimal coverage of the struts has occurred, which precludes potential embolization of the degrading scaffold. The subsequent restoration and resorption phases end with the final resorption [14].
Consequently, a shift is expected into biodegradable scaffolds, especially after the first BRS, Absorb GT1 (Abbott, USA), had been approved by the Food and Drug Administration (FDA) in 2016. Due to this development, abundant studies have been carried out in this field, showing mixed results regarding superiority. Several studies exposed positive outcomes regarding biodegradability, early restoration of the vessels function [15], improved post-procedure region [16] and lower angina [17]. Conversely, the studies showed comparable results between BRS and DES regarding acute recoil [16], target lesion vascularization [18], lumen area [19] and eccentricity index. Still, the main limitation that hampers the successful development of BRS is the material performance of degradable polymers, and corrodible metals [20][21]. Development and progress on specific capabilities have revealed and emphasized shortcomings in other domains.

1.3. Additive Manufacturing in bioresorbable stents

In addition to the above-described developments in design and material selection, to pursue the creation of an ideal stent, there must also be attention to manufacturability. The current fabrication technique used for BRS as the Absorb GT1 (Abbott, USA) and the DeSolve (Elixir Medical Corp, USA), consists of polylactic-acid (PLA) extrusion, after which it is lasered and post-processed to fulfil the medical standards [22]. The shortcomings of the above-described process are that it is time-consuming and expensive and only offers limited sizes and geometries for cardiovascular stent applications. Hence, there is a need to consider the manufacturing process related to both cost and patient-specific fit aspects. Additive Manufacturing (AM) is a formalized term for what used to be called rapid prototyping or 3D printing. Advances in AM have enabled the possibility of developing polymeric complex scaffolds and could potentially be a method to produce cardiovascular stents. Fabricating patient-specific devices is a benefit that endorses the use of AM [23][24][25][26].

Currently, numerous AM techniques are available on the market, but all with specific properties and possibilities. Extrusion- and photopolymerization- based printing methods and powder bed fusion are the AM techniques that are widely studied for the manufacturing of biomedical devices. Photopolymerization-based methods, such as Steriolithography (SLA), are often chosen as a manufacturing technique for high precision customized purposes [27]. Research by Cortes (2017) [28] compared various 3D printing techniques and endorsed the selection of SLA over extrusion-based printing methods (e.g. fused deposition modelling) (Appendix A). SLA uses a liquid photopolymer which is (layer-wise) polymerized by selective delivering energy (UV light) to create specific areas of a partial cross-section (Figure 1.2) [29]. Higher control over surface smoothness and surface finish bring highly favourable benefits when working with such small dimensions used for cardiovascular stents. Still, the biggest drawback is the limited number of biopolymers available for this method. Mainly because the pre-resin should include (a) a low molecular weight (Mw) and (b) desirably no crystallinity in order to reduce its viscosity [30]. Besides, there is a need for biocompatible acrylates (initiate crosslinking of polymers) [31].

Despite the limitations mentioned above, SLA has been used as a technique for the fabrication of tracheobronchial stent by Lim et al. [32]. Moreover, research continues, and new techniques are continuously being developed. For example, all three methods mentioned above require point-by-point material scanning, which leads to inhomogeneous structural properties and long production times [32][33]. Projection micro stereolithography (PμSL) tackles the low throughput problem by projecting UV light patterned by a dynamic mask in order to photopolymerize an entire cross-sectional layer in one exposure [33]. Thereby, PμSL technique was improved by adding an oxygen-permeable window plus a constantly moving build substrate, so-called continuous projection micro stereolithography (μCLIP). CLIP showed promising results regarding its possibilities to create 3D geometries at relatively high speed with uniform mechanical properties and good surface finish, which are the main obstacles for current AM technologies [34]. Ware et al. [35] continued with the development of μCLIP to improve the resolution to print on micron-scale precision. The researchers succeeded in reducing the fabrication time from a few hours to only a few minutes, including more uniform mechanical properties and even better surface finish than other AM techniques. As a result, a customizable bioresorbable stent has shown similar mechanical properties to existing metallic stents.

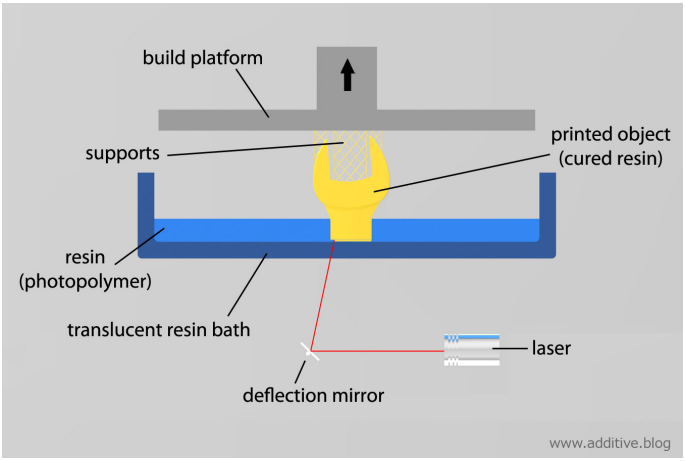

Figure 1.2: Schematic rending of stereolithography (SLA) [36]

Conclusively, there is an insistent need for new fabrication methods due to the current time consuming and expensive manufacturing process. In addition, it only offers limited sizes and geometries for cardiovascular stent application. If the standardized dimensions of the stent do not match the specific patient vascular size, the therapeutic outcome will be affected due to vessel rupture (too large diameter) or poor adherence, and thus displacement (too small diameter), resulting in added suffering for the patient and higher costs [37]. Moreover, due to the significant importance cardiovascular stents fulfil in world health, it is essential to be innovative and generate high quality, affordable medical devices. SLA could potentially be a method to accomplish these goals. However, data on the actual implementation of SLA as a novel manufacturing technique (regarding morphology, dimensions, design, degradability, geometry and materials) still is limited and

considered a research gap. Subsequently, AM (e.g. SLA) as a fabrication method for BRS is in an unexplored stage, which allows for diverse developments and research. A complete turnaround in the whole stenting intervention process is expected (Figure 1.3).

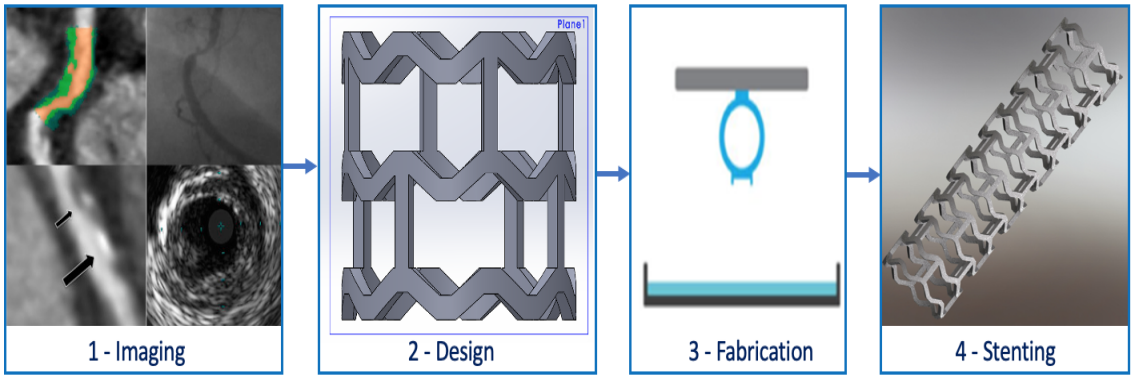

Figure 1.3: Vision on novel stenting intervention process: step 1) state-of-the-art imaging modalities will assess patient specific cardiovascular parameters, 2) based on obtained parameters, computer aided design file (CAD-file) (biomaterial, dimensions, geometry, drug release profile) is attuned, 3) the personalized BRS is fabricated on-the-spot using SLA, 4) customized BRS is ready for delivery and deployment.

1.4. (Bio)materials

The choice of material and processing routes are of significant importance to the structural and mechanical characteristics of the stent. Subsequently, material selection is inherent to the main limitations (resorption time, strut thickness, recoil, fracture risk and deliverability), hampering the path of BRS to become a mainstream technology.

Over recent years, the interest in the synthesis of biodegradable metals and polymers has increased and focused on new materials in regenerative medical science. Generally, metals have the advantage of a high radial force, resistance to fracture, biocompatibility, radiopacity, low thrombogenicity and flexibility. Presently, available metallic biomaterials for the fabrication of stents include Cobalt-Chromium (CoCr), 316L Stainless steel (SS), Platinum chromium (PtCr), titanium and nitinol [38]. Despite the nontoxic levels of free metals upon resorption, there is a risk of oxidative stress-inducing levels of transition metals, causing excessive inflammation and vasomotor dysfunction at the stent site [39]. Thus, the prime reason to switch to bioabsorbable polymers is the potential to decrease chronic inflammation and improve vascular healing [20][21]. Additionally, maintaining suitability for possible future therapeutic options (e.g. in the case of multivessel disease), as well as the restoration of natural vascular physiology (of the stented segment), are notable advantages [40]. Conversely, polymers suffer from restricted distensibility, risk of strut fracture, low radial and tensile strength, maintaining adequate strength and thickness of strut [41]. Although optimization remains a point of further development, this research focuses on polymer cardiovascular bioresorbable stents fabricated by stereolithography.

The polymer BRS generally consists of Polylactide acid (PLA), Poly(ϵ -caprolactone) (PCL), Polyglycolic acid (PGA) or a combination [22]. PLA is polyester and the most used biomaterial in BRS because of its bioactive and biodegradable characteristics, comprehensive research, and the proven track record regarding successful *in vivo* biomedical applications [42]. Generally, it is synthesized via the ring-opening polymerization of the cyclic dimers of lactic acid for healthcare purposes. The polymerization of L or D-lactide results in isotactic poly (L- lactide) (PLLA) or poly(D-lactide) (PDLA), though polymerization of the monomer (D, L-lactide) results in atactic amorphous polymer poly (D, L-lactide) (PDLLA) [43]. Furthermore, chemical modification of the physical properties and biodegradability of PLA is attained through copolymerization or by the racemization of D- and L-isomers. PLLA is a semi-crystalline polymer and offers much versatility and therefore is widely used in the treatment of CAD. It ultimately degrades carbon dioxide and water. Compared to metallic biomaterials as CoCr, PLLA experiences lower tensile strength, ductility and stiffness [44]. As a result, PLLA stents have to compensate by thickening their struts and widening their strut profile. Nonetheless, the tensile

and radial strength is only half of the rates of metal stents [45]. Due to the -above described- mechanical and chemical properties, PLA is a suitable option for BRS. Besides, the Absorb GT1 (Abbott, USA) was comprised of a PLLA backbone coated with PDLA.

The biomaterials described below are still in the research stage/clinical trials to prove their BRS functionality. PCL is a biocompatible and semi-crystalline polymer with a considerably longer degradation time than PLA. To modify material properties, PCL can easily be copolymerized with other polymers. Furthermore, PCL gained recent popularity through the easiness of production as it has multiple appealing features in its viscoelastic and rheological properties over various aliphatic polyester counterparts [46]. For example, poly(L-lactide-co-ϵ -caprolactone) is a copolymer developed to add flexibility to the building material of a structural device. Besides, copolymerization of lactide with caprolactone can be helpful for control of degradation rate, shape-memory behaviour, controlled drug release and mechanical properties, which widens the PLLA biomedical application potential. By shuffling the amount of incorporated caprolactone (CL) in the lactide- caprolactone copolymer, researchers can vary the brittleness of PLCL compared to PLLA (homopolymer). CL enables the lowering of the Transition temperature (Tg) and thus reduce the material stiffness [47]. Polyurethanes (PU) are particular groups of elastomeric block copolymers, which are comprised out of semi-crystalline segments (hard) and rubbery segments (soft). On the one hand, a diisocyanate component and a diol or diamine (as chain extender) contribute to the hard segment. On the other hand, flexible and reasonably long components (polyester or polyether) are used to enhance the soft segment [48][49]. Over recent years, PUs containing a broad chemical diversity has gained increasing interest in biomedical fields. Primarily due to their flexibility and variable mechanical characteristics [50].

To finalize, all above-mentioned (bio)materials contain both positive and negative properties. However, since SLA has been selected as a manufacturing technique, the prospective Biomaterial ink (B-ink) should encompass all SLA bounded resin requirements, as stated in paragraph 1.3. First of all, SLA uses (layer-wise) continuous polymerization of photosensitive polymers to develop the requested object. Photosensitive polymers react when exposed to (UV) light and as a consequence they crosslink [51]. For crosslinking to occur, photocurable moieties (e.g. multifunctional epoxy or acrylate monomers) are required. The curing of (meth) acrylates is established through radical chain-growth polymerization during the printing process, while epoxy resins are done using a step-growth manner when anhydrides or amines are available in its environment [52]. These photocurable acrylates consist of multiple components such as (a) monomers (basic building blocks of polymers), (b) crosslinkers (molecules that can bind two or more polymers together), (c) photoinitiators (to start the reaction) and (d) plasticizers/ fillers (get tangled into the polymer matrix and prevent shrinkage of the model). To enhance the printability and resin characteristics, stabilizers and optical absorbers are added as well. The latter, due to the sensibility of SLA printers. Slight variations in viscosity, molecular weight or other parameters can have an enormous effect on the success rate of the print. Secondly, all single chemicals involved in the composition must be biocompatible in any state of matter. Thirdly, it is important to note that the SLA printing of bioscaffolds still is in its pioneer stage and resin composition characteristics acquire a precise and essential role in the success rate of a print. To the best of the authors' knowledge, there have been only several attempts to explore the potential of SLA three-dimensional BRS printing [39][35]. The Hague University of Applied Sciences explored the possibility of 3D printing BRS involving (partly) biocompatible materials. Van Lith et al. [39] established to develop a 3D-Printing strong high-resolution bioresorbable vascular stents. The study mainly focused on the stents' radial strength, and thus the researchers selected a rigid component. Because of the high sensitivity of SLA printing, the non-biodegradable (commercial) resin will disclose SLA restraints as a fabrication method for cardiovascular stents, while the biodegradable composition of van Lith et al. [39] is mimicked to ensure successful printing. However, flexibility is an essential parameter to enable deliverability and so, subsequent to the simulation of the existing protocol, certain specific adjustment involving the flexibility of the stent are inserted.

1.5. Significance of study

1.5.1. Problem statement

Cardiovascular stents are positively contributing to global health. The main reason to switch to bioresorbable polymers is the potential to decrease chronic inflammation and improve vascular healing. Since the first BRS, Absorb GT1 (Abbott, USA), was FDA approved, a new shift was expected towards bioresorbable scaffolds. However, structural and mechanical limitations of the current BRS are hampering the path to become

a mainstream technology. The current time-demanding stent fabrication process suffers from low efficiency and high costs and only offers limited sizes and geometries for cardiovascular stent application. Patient-specific bioresorbable cardiovascular stents could potentially improve vessel patency because of (a) optimal sizing averting malaposition, (b) an adequate coupling between the plaque's geometry and the stent, and (c) optimal design in terms of degradation, strength, drug loading and release profiles. Hence, there is a substantial need for 'patient specific' cardiovascular BRS. The employment of AM (e.g. SLA) is still in an exploratory stage, including complete diverse research and development, focusing on factors that hinder the implementation of SLA as a suitable manufacturing technique, such as poor mechanical properties, low accuracy and quality. However, SLA could potentially be a manufacturing process to fabricate these medical devices. The corresponding process parameters have a significant effect on the minimization of the previously mentioned shortcomings. Hence, it is essential to understand how process parameters affect the morphological and mechanical characteristics of models. The printing layer thickness is identified as the most influential process parameter and will be investigated in this research.

1.5.2. Research objectives

Moore et al. [53] stated that when a stent can be manufactured using a singular machine, in approximately 20 minutes, the genuine possibility of creating fast on-the-spot and on-demand printing of patient-specific bioresorbable stents can be achieved. Thus, the goal of this research is to provide novel data on the subject. Therefore, this thesis will:

- Investigate the printability of cardiovascular stents using SLA as the manufacturing technique
- Optimize insights concerning the SLA printing limitations regarding support structure, dimensions, printing direction and repeatability in multiple stent dimensions
- Explore how the printing layer thickness affects the mechanical and morphological characteristics of the stent
- Analyze the stents' morphological characteristics regarding surface finish, surface roughness and cross-section structure
- Quantify surface roughness and printing accuracy
- Provide a mechanical analysis focusing on radial strength, viscoelastic effect, cyclic loading, tensile strength and longitudinal compression

1.5.3. Aim of the study

This study aimed to investigate the possibilities to 3D-print a polymeric cardiovascular bioresorbable stent prepared by stereolithography that offers adequate morphology and mechanical properties for clinical applications.

2

Materials and Methods

2.1. Stent design

Generally, the structure or design of a stent comprises scaffolding, which includes a network or specific pattern of interconnecting structural elements (struts). These struts typically consist out of a sequence of sinusoidal hoops linked by several connectors. These elements can be divided into several parameters, such as strut width and strut thickness. Besides, the diameter of the stent is an important parameter as well. All -above mentioned- parameters are demonstrated in Figure 2.1.
As previously stated in section 1.2, the Absorb GT1 (Abbott, USA) was the first, and only FDA approved BRS (2016). Subsequently, the author aimed to mimic the design of the clinically proven Absorb GT1 (Abbott, USA). Parameters and dimensions were provided from the FDA Review by Kenya Brothers [14]. The design (Appendix B) was rendered with SolidWorks (Dassault Systèmes SolidWorks Corp., USA) involving several deviations varying in strut thickness and diameter (CAD files upon request). The Absorb GT1 (Abbott, USA) contained a strut thickness of 150 µm linked to varying diameters. All requisite mechanical tests were performed on 3 mm (outer diameter) scaffolds [14], and so, multiple stents were obtained with an outer diameter of 3 mm, and varying strut thicknesses between 100 – 200 µm. Research on SLA fabricated cardiovascular stents was limited. Only several studies presented scaffolds with an outer diameter of 4 mm and a strut thickness of 200 µm [28] [39].

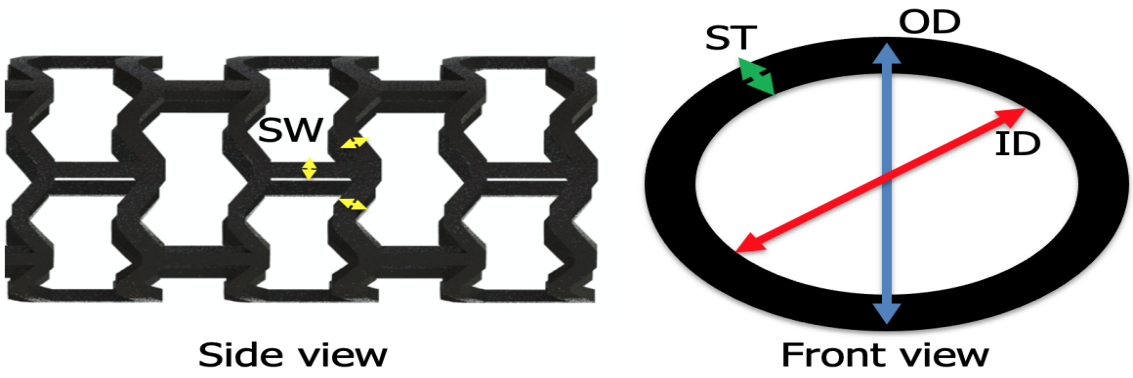

Figure 2.1: Schematic representation of the essential parameters of a stent. The side view demonstrates the strut width (SW), where the front view shows the strut thickness (ST) and (inner and outer) diameter (IN/ OD) clearly.

2.2. (Bio)material selection

The research focused on two (bio)materials, (a) a non-biodegradable resin and (b) a biodegradable variant. The commercial non-biodegradable resin was selected due to its accurate composition for the corresponding 3D printer containing the correct printing settings. Last mentioned, is a crucial aspect to fabricate a successful print. The biodegradable resin was utilized to investigate the possibility of 3D fabricating a cardiovascular

stent involving acceptable morphological and mechanical properties for clinical use. It is important to note that primarily the protocol of van Lith et al. [54] was followed as a guideline to develop a biodegradable resin. In this context, the term 'biodegradable' resin, or B-ink, was adopted from the corresponding literature. Additionally, the two types of resin were compared on the previously mentioned properties to analyze any potential difference between a (commercial) optimal and a (non-commercial) substandard resin.

2.2.1. Non-bioresorbable resin

A commercial device (Form 3, Formlabs, USA) was deployed to explore the limitations of SLA printing regarding dimensions and support material, using their Grey Resin V4 1L (Formlabs, USA). The printing settings, such as initial layer height, initial exposure times and standard exposure times, are already optimized for the commercial resins, making it ideal for exploring the earlier mentioned limitations of SLA. The resin is proprietarily composed of Urethane Dimethacrylate 55-75 wt. %, Methacrylate Monomer(s) 15-25 wt. % and Photoinitiators <0.9 wt. % [55]. Despite limited information available on all available resins, the Grey resin was selected due to its ability to print a wide range of layer thicknesses (LT), high Ultimate Tensile Strength (65 MPa) and relatively low costs.

2.2.2. Bioresorbable resin

Synthesis: Citric acid and 1,12-dodecanediol were melted (165 °C, 15 min) in a 2:1 ratio, respectively. Involving 12 g 1,12-dodecanediol (mw: 202.33 g/mol) and 22.79 g Citric acid (mw: 192.12 g/mol). Co-polymerized (140 °C, 30 min) and purified. The prepolymer (22 g) was dissolved in a mixture (180 mL tetrahydrofuran, 816 mg Imidazole and 17.04 g Glycidyl methacrylate), heated (60°C, 6 hr) and purified to yield mPDC. The formulation of the B-ink involved 47.8% mPDC, 2.2% Igracure 816 (photoinitiator), 0.08% Sudan I (UV absorber to control curing depth) and 50% Diehyl fumarate (to control viscosity). The resin was set to mix (50 °C, 1 hour) and left stirring afterwards for 48 hours more, ensuring homogeneity.
Polymer Characterization: H nuclear magnetic resonance (^{1}H NMR) spectra for (pre)polymers were recorded each step on a ^{1}H NMR spectrometer (Spinsolve 60MHz carbon, Magritek, Germany) at 15 MHz. The ^{1}H-NMR spectra were referenced relative to van Lith et al. [39]. The (pre)polymers were purified via cooling the (pre)polymer down to RT, solved in 200 mL ethyl acetate, after which 500 mL ddH_2O was added while stirring. The whole was added into the separatory funnel and extracted 3x with 150 mL batches of ethyl acetate. Combined ethyl acetate layers were stirred up, and 300 g Na_2SO_4 o/n. Filtration was performed by evaporation using a Rotavapor (30 C, 75 rpm, o/n). All spectra were obtained at RT from solutions of 0.7 mL of deuterated chloroform ($CHCl_3$).

2.3. (m)SLA

As previously stated in section 1.3, SLA (photopolymerization-based method) was selected due to its high precision and higher control over surface smoothness/ surface finish, which brings benefits that are highly favourable when working with small dimensions. The biggest downside is the limited biopolymers available for this method. The Form 3 (Formlabs, USA) was the available SLA printer at the TU Delft (Delft, The Netherlands) for the procedure of the non-biodegradable resin (Grey resin V4 1L, Formlabs, USA). The Form 3 printer uses a laser unit that directs a UV beam to a reflective mirror, from where a Galvo motor system stirs the focussed beam to the resin's surface. Subsequently, the solidification will occur via a layer-by-layer printing process. These layers have a thickness, the so-called 'layer thickness'. The latter is a measure of the layer height (z-axis) of each successive addition of material in the SLA printing process in which layers are stacked. It is one of the essential technical characteristics of layer-by-layer 3D printing methods. Only commercial resins were suitable for this printer, and thus, the Prusa SL1 (Prusa Research, Czech Republic), available at the Hague University of Applied Sciences (The Hague, The Netherlands), was used to print the B-ink resin. The Prusa SL1 is a masked SLA (mSLA) 3D printer that performs solidification by exposing a high-performance UV LED, which cures whole layers simultaneously, while a masked screen filters out light for a particular area shape.

2.3.1. Stent fabrication with the Form 3

The CAD model (STL file) was uploaded in the accessory software PreForm (Formlabs, USA). The models were replicated multiple times per print. Printing was performed with varying layer thickness resolutions (25, 50, 100 and 160 μm), a support density of 1.00, a support touchpoint size of 0.10 mm and shifting inclination angles concerning the printing bed. The latter was determined per inclination angle by a continue-to-failure

structure, implicating an increase in the number of samples (by one) after a successful print. The process continued until failure, after which it was repeated (3 times total). The non-biodegradable resin (Grey resin V4 1L, Formlabs, USA) was decanted in a clean Resin Tank V2 (Formlabs, USA) while averting contamination and exposure to sunlight. The corresponding print settings were selected, and the printing process was initiated. The samples were obtained after a printing time of ~ 24 min – 109 min, depending on the selected layer thickness. After removal from the building platform, the samples were carefully washed for 10 min in a 2-propanol (Sigma-Aldrich, USA) using a pair of tweezers. Subsequently, the samples were prudently air dried with compressed air for 2 min, followed by removal from their mechanical support structures. Lastly, the samples were post-cured using a UV flood exposure system (Form Cure, Formlabs, USA), fluctuating from 0, 5, 10, 15, 20, 25, 30, 35, 40, 45, 50, 55 and 60 min. The samples were stored in glass vials covered with Aluminum to prevent further UV curing.

2.3.2. Stent fabrication with the Prusa SL1

The CAD model (STL file) was uploaded in the accessory software PrusaSlicer (Prusa research, Czech Republic). Printing was performed with a layer thickness resolutions of 25 µm, a support density of 1.00, a support touchpoint size of 0.10 mm and an inclination angle of 45 degrees with respect to the printing bed. The B-ink was decanted in a clean resin tank while averting contamination and exposure to sunlight. Additionally, the building platform was clean thoroughly with 2-propanol (Sigma-Aldrich, USA). Print settings were adjusted involving an exposure time of 35 seconds and a preheated resin of 50 °C. The samples were obtained from the building platform and carefully washed for 10 min in 2-propanol (Sigma-Aldrich, USA) and dried using the Original Prusa Curing and Washing Machine (CW1) (Prusa Research, Czech Republic). Subsequently, the mechanical support structures were removed, and the samples were post cured for 45 min, using the CW1. The samples were stored in glass vials covered with Aluminium to prevent further UV curing.

2.4. Stent (structural) characterization

The (structural) characterization was divided into (a) morphology analysis, (b) mechanical investigations and (c) structural analysis. The non-biodegradable resin stents were analyzed on the sector a and b, involving a strut thickness of 200 µm and fabricated using different layer thicknesses. Lastly, the B-ink variant was structural characterized (c) using ^{1}H-NMR to eventually be exposed to all similar analysis performed on the non-biodegradable resin samples, as deliberated above.

2.4.1. Morphological analysis

2.4.1.1. Scanning electron microscopy

The JSM-IT100 InTouchScope (Jeol, Ltd., Japan) scanning electron microscope (SEM) was adopted to analyze the stents' strut thickness, diameter, surface roughness and cross-section. The experiment was performed with an electron beam energy of 10 kV, the working distance varying from 10- 28 mm and chamber pressures of 60 Pa in a High Vacuum (HV) setting. Due to the polymeric composition of the stents, low visibility is expected among the SEM. Also, when analyzing non-conductive samples in conventional, HV mode, a very thin conductive layer is required to protect the samples to prevent charging and heating of the sample. Consequently, the sputter (JFC-1300 Auto Fine Coater, Jeol, Ltd., Japan) was used for 60 seconds to conduct a very thin layer of conductive gold. The imaging mode Secondary Electron Detector (SED) was used to obtain all topographic SEM images. These images involve a high resolution independent of the material and acquired from inelastically scattered electrons close to the surface. Prior to imaging, the samples were washed using 2-propanol (Sigma-Aldrich, USA) and deionized water for 60 seconds, followed by compressed air drying. Various analysis and measurements were performed to analyze the morphology. First, a surface analysis was performed investigating the influence of the printing layer thicknesses on the surface morphology. Secondly, the cross-section structures of the samples were analyzed by initiating a crack in both the transverse plane as the sagittal plane. Thirdly, the SLA-printed samples' accuracy was examined by measuring the strut thickness at eight specific points (Figure 2.2) and evaluating the outer diameter. The stents consist of round structures, where the 'accuracy' imaging occurs from above (proximal side), initiating an angle and thus inevitably creating inaccurate results. The proximal section corresponds to the area closest to the printing bed. Therefore, to minimize the angle, the stent's length was attuned in SolidWorks from 10 mm to 3 mm, and subsequently, 3D printed. All SEM experiments were performed after post-processing of the 3 mm diameter stents. Moreover, an increased number of 10 samples per variant per experiment were analyzed to check the intra-user dependency.

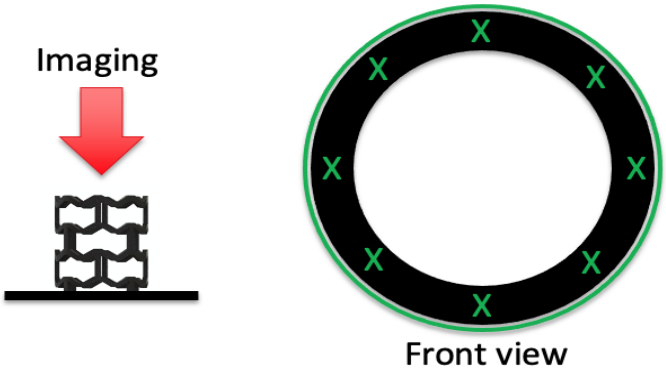

Figure 2.2: Representation of the measurements recorded during the SEM analysis of the stents. The stent strut thickness and diameter were obtained from a front view, only the proximal area was taken into account. The strut thickness was measured at eight (X) similar points at each sample.

2.4.1.2. Interferometer

Surface roughness is quantified by the deviations in the direction of the normal vector of a real surface from its ideal form, using the system ContourGT-K white light optical profiler (Bruker Corporation, USA). Topographical characterization of 4 gold-sputtered flat samples fabricated with 25 µm, 50 µm, 100 µm and 160 µm layer thickness was performed. The vertical scanning distance was set at 100 m. There were four measurements of 300 x 292 m size performed on each sample, as depicted in Figure 2.3-b. The roughness of the samples was assessed in the Gwyddion software by applying tilt correction and polynomial levelling. The roughness profiles were exported both as line graphs and colour-mapped 3D representations. There are several roughness parameters feasible, where R_a is the most commonly used. R_a is the arithmetical mean deviation of the assessed profile and described in the formula 2.1 described below.

$$R_a = \frac{1}{l_r} \int_0^{l_r} |z(x)|\, dx \tag{2.1}$$

The interferometer makes use of waves that are superimposed, causing the phenomenon of interference. This phenomenon is used to extract data on the roughness of the stents. The interferometry was deployed to analyze all configurations, after which the Atomic Force Microscope was used to verify the Interferometer results.

2.4.1.3. Atomic Force Microscopy

The Atomic Force Microscope (AFM) was deployed to verify the Interferometer results. Topographical characterization of one flat sample fabricated with 25 µm layer thickness was performed using AFM (Figure 2.3-a). The system used was the JPK NanoWizard 4 (Bruker Corporation, USA), with a TESPA-HAR probe (Bruker Corporation, USA). The cantilever had a width of 40 m, a length of 125 m and a nominal spring constant of 37 N/m. The tip had a nominal radius of 7 nm, and it was manufactured out of antimony doped Si. Probe calibration was performed using the thermal method. The topographical image of the 3D printed surface was acquired in QI mode, with the following parameters: setpoint 200 nN; z length 15 m; pixel time 6.8 ms. A 100 x 100 m area was scanned on one 3D printed flat sample with a layer thickness of 25 m. The roughness of the sample was assessed in the JPK Data Processing software (Bruker Corporation, USA) and exported as a .png image containing the height values.

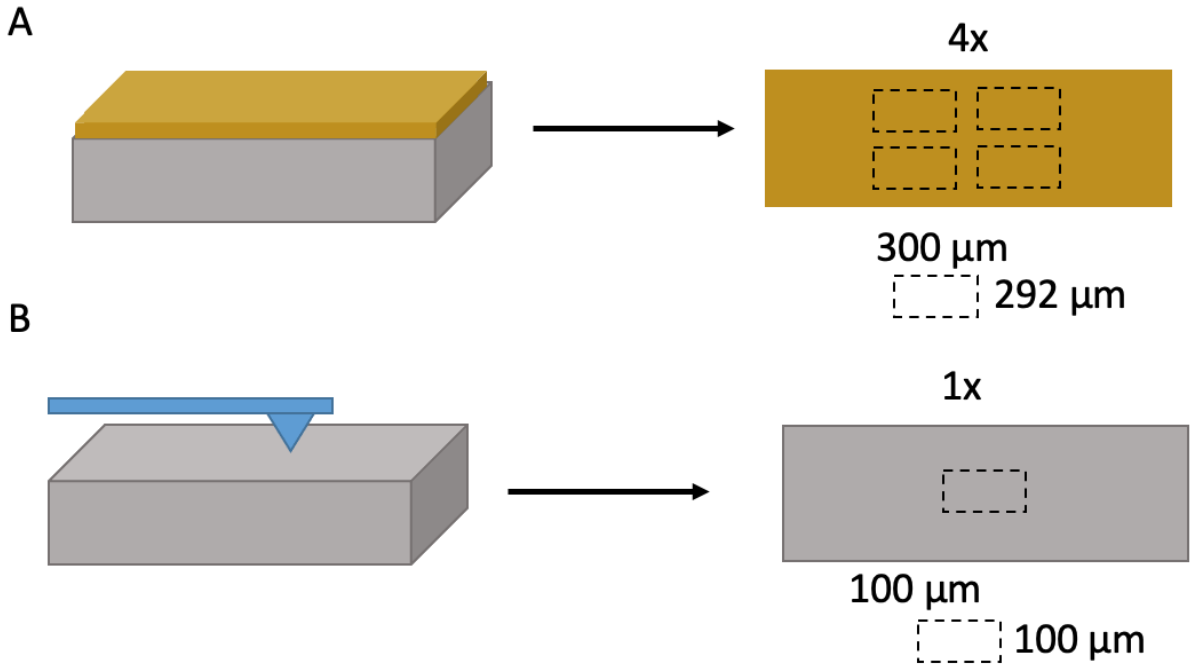

Figure 2.3: A: Graphical Representation of AFM measurement on the 3D printed flat sample. B: Graphical Representation of white light interferometry measurements on 3D printed gold-sputtered flat samples.

2.4.2. Mechanical analysis

2.4.2.1. Radial compression

The main and initial function of a stent is to support the dilated vessel and prevent (partial) prolapse of tissue. In this context, radial compression tests are essential, and a measure for crush resistance of stents [56]. Therefore, to investigate the ability of the stents to endure the loading force from the lesioned vessel, compression tests were performed. There is no straight answer of what value radial compression resistance is sufficient. Ware et al. [39] tested the mechanical performance of a currently used Bare metal stent (BMS) coronary stent. This expanded stent showed a 1.03 N load at 25% radial compression. Subsequently, this value has been set as a minimum required value on radial strength. The experiment was performed at various time points (0, 5, 10, 15, 20, 25, 30, 35, 40, 45, 50, 55 and 60 min) after post-processing and involved stents that were placed horizontally in a compression machine (Lloyd LR5K, Ametek Inc., USA) exploiting a 5 N load cell. Compression was deployed at differing deformation rates (0.2, 0.5, 1.00, 1.25, 1.50, 1.75, 2.25 and 2.75 mm/s) up to a 25% compression of the stent's diameter, subjected to a constant load in the y-direction (Figure 2.4). The particular deformation rates are equivalent to 8, 20, 40, 50, 70, 90 and 100 bpm, respectively. Initially, the radial resistance at maximum compression was measured. Furthermore, to assess the elastic behaviour of the stents, the samples were radially compressed over one cycle (load-unload) to account for potential viscoelastic effects on compression behaviour. Three samples of the 3-mm diameter stent of each configuration were tested.

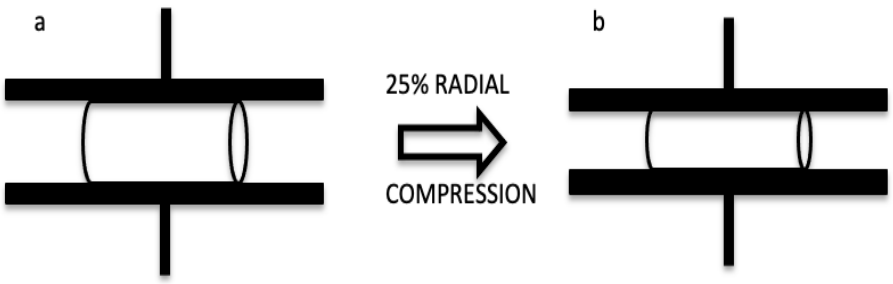

Figure 2.4: Schematic diagram of mechanical testing setup for radial force experiment. (a) Stent at 0% compression, (b) Stent at 25% compression from a load in the y-direction.

2.4.2.2. Cyclic loading

The stents' long-term recovery potential was analyzed by applying successive cyclic radial 25% deformations (from 4200 up to 67200 cycles) at a 1.75 mm/s deformation rate. A sinusoidal function of displacement was used to mimic pulsatile arterial pressure and defined as a dynamic loading group. The radial strength was plotted as the change in diameter as a function of uniformly applied external radial pressure. The experiment involved stents placed horizontally in a compression machine (Instron Electropuls E10000, Instron, USA) exploiting a 10 kN load cell. Three samples per configuration were considered for all tests.

2.4.2.3. Tensile testing

A cylindrical tensile bar comprising a stent in the middle section was developed to determine the tensile properties of the stent by uniaxial tensile testing. A SolidWorks simulation was deployed to determine if the load distribution within the tensile bar was accurate (Appendix C). Figure 2.5 represents the shape and dimension of the tensile bare used for tensile testing. The experiment involved tensile samples placed vertically in a tensile machine (Lloyd LR5K, Ametek Inc., USA), exploiting a 5 N load cell with a transverse rate of 1 mm/min. Stress and strain behaviours of the prepared samples were used to calculate the elastic modulus. Three samples per configuration were considered for all tests.

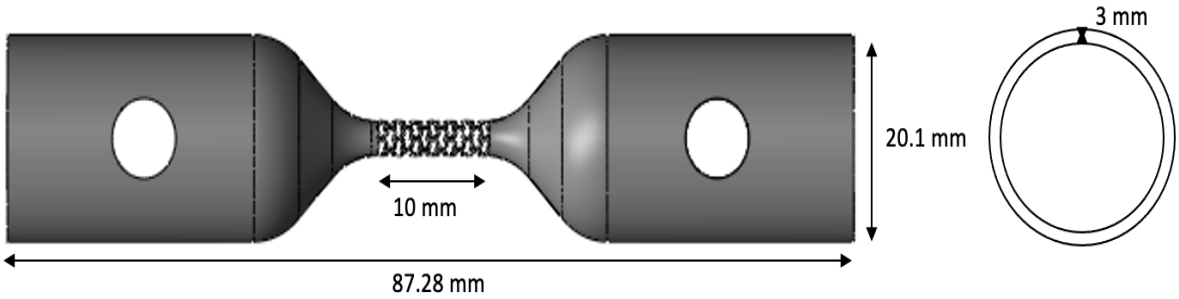

Figure 2.5: Schematic display of stent customized tensile specimen including corresponding properties.

2.4.2.4. Longitudinal compression

Recent clinical observations showed significant longitudinal compression or 'stent shortening' in several contemporary stents, which occurs during the re-crossing with other devices such as stent delivery systems, post-dilatation balloons, or catheters [57][58]. A clinically relevant longitudinal compression force was estimated, to which a stent could possibly be subjected in a case when a catheter tip is caught while crossing a stent. This force was determined to be 50 gram force (0.49 N) [57]. The stents were placed vertically between two direct parallel plates (Lloyd LR5K, Ametek Inc., USA) to explore its longitudinal crush resistance. All samples were subjected to a longitudinal compression force of 0.5 N y-direction). The longitudinal deformation at the specified load was measured using a 5 N load cell at 1 mm/min. The experiment was conducted on 3 mm diameter stents, and three samples of each model were analyzed.

2.4.3. Resin viscosity analysis

Resin viscosity is an essential parameter of the SLA printing technique that can significantly impact the printing success rate. These viscosity's should be within the margin range of 35-4000 mPa·s for all SLA printable resin viscosity's [59]. The MCR 302 (Modular Compact Rheometer, Anton Paar, Austria) was deployed to measure the shear viscosity at a constant shear rate. A volume of 5 mL was decanted on the plate, after which the spindle dropped down on the resin. Subsequently, the spindle rotated with a constant shear rate of 50 1/s for 120 seconds.

2.5. Statistical analysis

The statistical difference between each (layer thickness) configuration (four groups) was analyzed using several tests. The Kruskal Wallis H tests (non-parametric alternative for one-way ANOVA) was used for experiments involving (three stents per group, four groups). If the sample sizes of specific experiments were greater than 20, a test of normality (Kolmogorov Smirnov) was performed beforehand. The Bonferroni correction for multiple tests has adjusted significance values. The analysis was performed in SPSS (IBM, USA) software. A statistically significant difference was distinguished by $p < 0.05$.

3

Results

3.1. Stent fabrication

3.1.1. Non-biodegradable stents

Printing of the stents was obtained with standard 'Grey resin' Form 3 (Formlabs, USA) parameters. Printing iterations entailed finding (a) the stent inclination angle with respect to the printing bed (Figure 3.1) and (b) the limitations regarding dimensions. The inclination angle was investigated to enhance the printing success rate and ease the release from the support material. The ultimate inclination angle (θ) was observed at 40 degrees, printing a maximum of four stents successfully (Figure 3.2). Total printing time varied between 24, 40, 52 and 109 min depending on the initiated layer thickness of 160, 100, 50 or 25 µm, respectively. Simulating the design of the Absorb GT1 (Abbott, USA), the strut thickness should be 150 µm, with an outer diameter of 3 mm [14]. This specific diameter was selected to normalize the obtained data as most studies reporting similar (mechanical) analysis used stents, including an outer diameter of 3 mm. The printing limitations regarding outer diameter and strut thickness were explored and displayed in table 3.1. To this extent, considering the set research goal to analyze the effect of the printing layer thickness, all successfully printed samples containing a diameter of 3.0 mm and strut thickness of 200 µm were selected for further characterization. The earlier mentioned strut thickness enables the feasibility of investigating four different configurations.

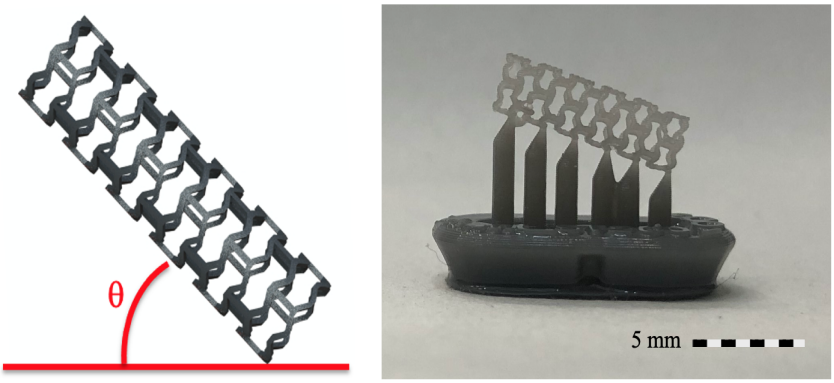

Figure 3.1: Schematic representation of the inclination angle of the stent with respect to the printing bed. To obtain the ultimate support settings for the Form 3 (Formlabs, USA), the angle θ was varied.

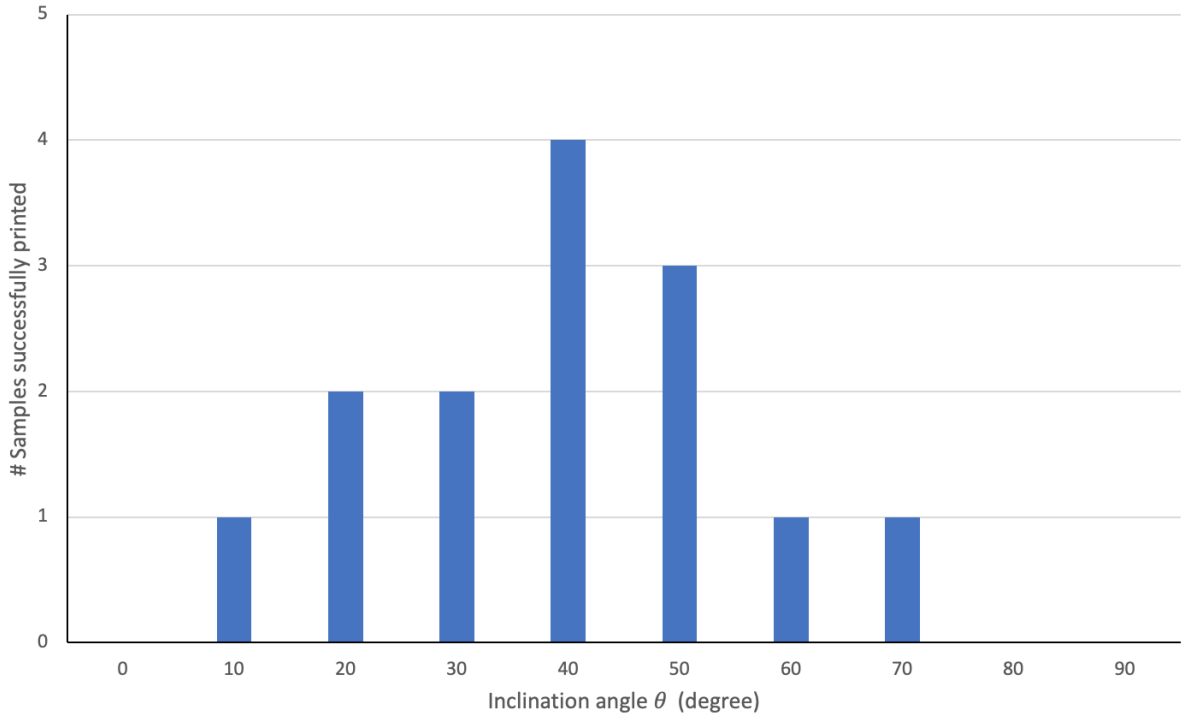

Figure 3.2: Number of successfully printed stents as a result of the inclination angle of the sample with respect to the printing bed, using the Form3 (Formlabs, USA). The highest success rate was observed between 40 and 50 degrees.

Table 3.1: Stents' (OD 3 mm) printing limitations concerning strut thickness. '✓' confirms the feasibility while 'X' indicates no successful print.

Non-biodegradable stents (OD 3 mm)		Strut thickness [µm]		
		100	150	200
Layer thickness [µm]	25	✓	✓	✓
	50	X	✓	✓
	100	X	X	✓
	160	X	X	✓

3.1.2. Biodegradable stents

3.1.2.1. Synthesis

Previous to the printing process, the B-ink was synthesized as described in section 2.2.2. The process consisted of a multiple-step procedure. First, the synthesis of methacrylated poly(1,12-dodecamethylene citrate) (mPDC), after which a ^{1}H NMR analysis was performed to confirm the polymers structure (Figure 3.3). Subsequently, mPDC was combined with a UV absorber and a photoinitiator to form the B-ink, which can be polymerized by exposure to UV light. The B-ink was exposed to a ^{1}H NMR to substantiate its final structure (Figure 3.4).

3.1.2.2. Structural analysis

The different signals of the ^{1}H NMR spectrum, shown in Figure 3.3, can be assigned and are compared to van Lith et al. [39] reference spectrum (Appendix D). The A gives the signal centred at 3.00 ppm, the signals around 3.75 and 0.75 ppm correspond to the B and the C, respectively, the signals at 5.75 and 6.25 ppm are the two hydrogens attached to the double bond from the methacrylate group (E), the signal at 2 ppm is the methyl group from the methacrylate (F) and the signal at 7.35 ppm is Chloroform. The rest in between are the 'in between' carbon atoms from the dodecandiol (D) and possibly some contamination. It is important to note that due to the use of Chloroform ($CHCl_3$) instead of dimethyl sulfoxide (DMSO) as solvent, a slight shift throughout the spectrum is expected. Moreover, the integral of signal G and H are 2.75 and 2.65, respectively, which indicates that the ratio is correct (two protons: two protons). Also, the integral of signal F, derived from

citric acid, is 5.53, which is almost similar to the sum of the integrals of G and H, implying a 1:1 mixture of the specific polymer.
Furthermore, the different signals of the ^{1}H NMR spectrum, shown in Figure 3.4, can be divided into a singlet at 6.9 ppm, a triplet at 1.5 ppm and a quartet at 4.4 ppm are derived from the ethyl fumarate. To be more specific, the singlet is derived from the fumarate, the triplet is from the methyl group, and the quartet originates from the CH_2. Moreover, the structure of both the mPDC and the B-ink was not as fluid as expected and required. Consequently, the resin did not contain the suitable characteristics regarding viscosity to initiate a 3D printing process.

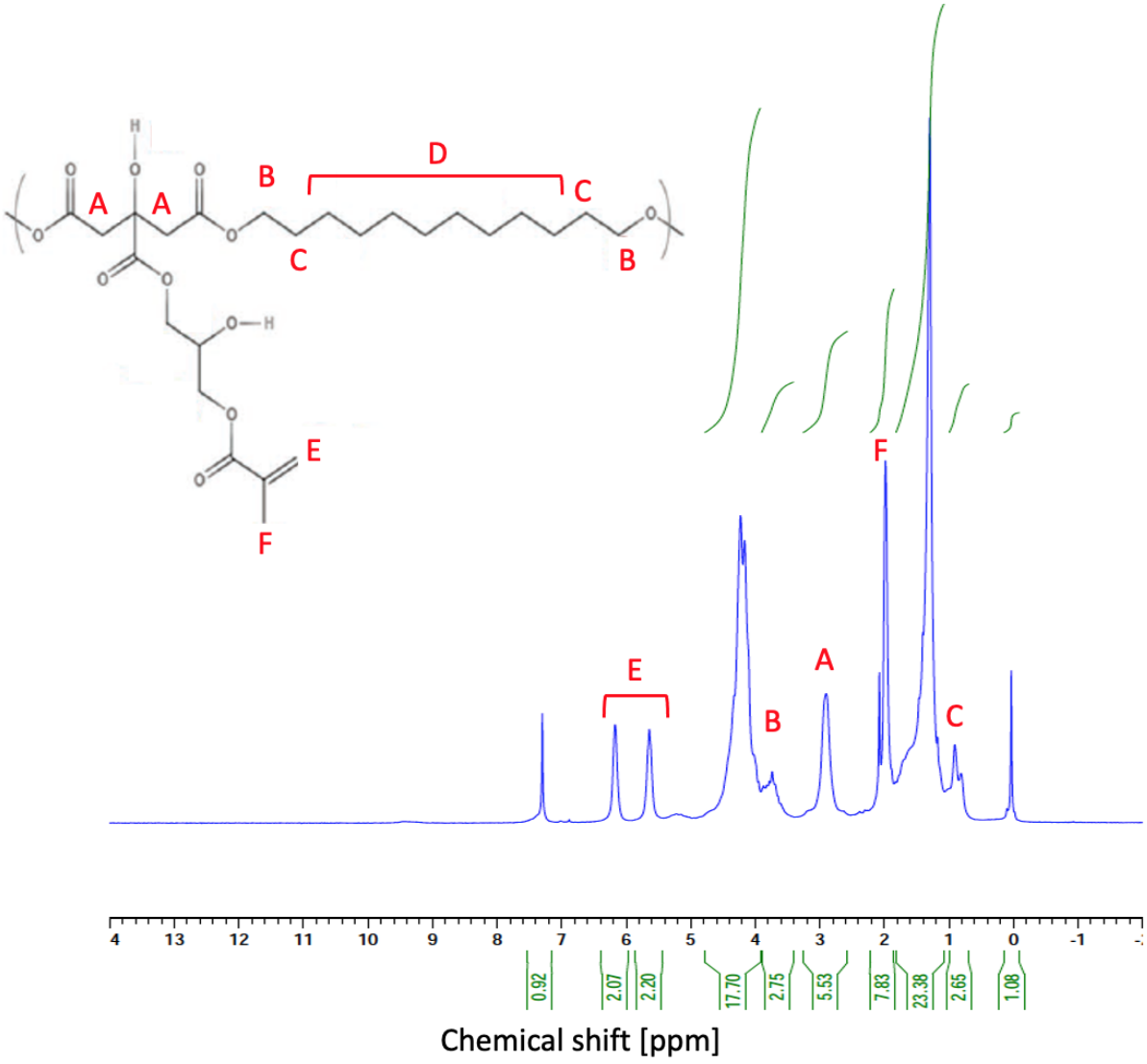

Figure 3.3: ^{1}H NMR spectrum of mPDC confirms its structure.

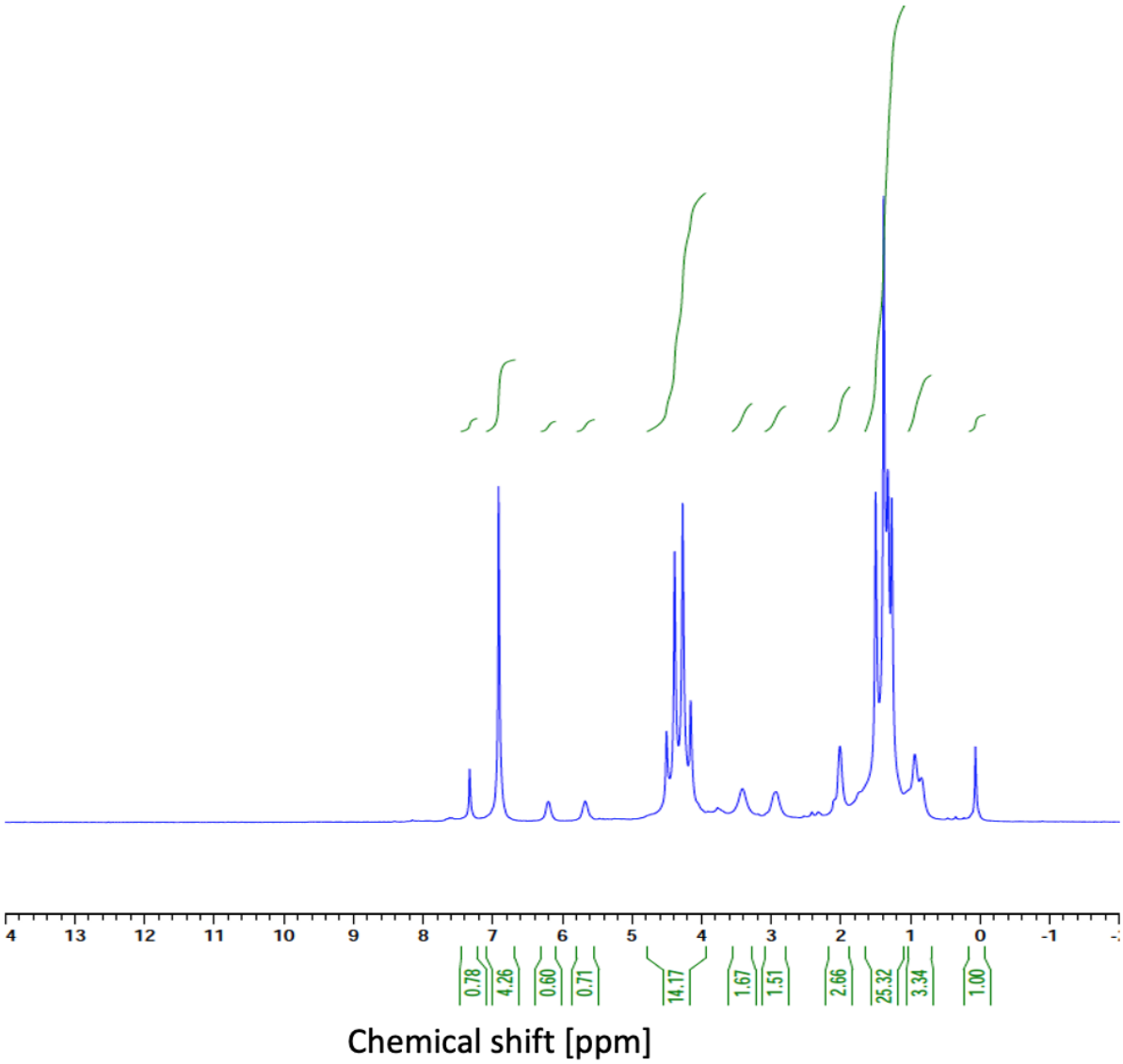

Figure 3.4: ^{1}H NMR spectrum of B-ink demonstrates its structure.

3.2. Stent characterization

3.2.1. Stent geometrical morphology

3.2.1.1. Surface morphology

The non-biodegradable printed samples were analyzed on surface finish, cross-section morphology and accuracy of various layer thickness resolution (25, 50, 100 and 160 µm) using the SEM. It is important to note that no obvious difference between the proximal, central and distal section of the stent was observed, where the proximal section corresponds to the area closest to the printing bed (Appendix E). Moreover, the selected layer thickness does show a direct link to the smoothness of surface morphologies. As observed in Figure 3.5, the stents printed with a 25 µm and 50 µm layer thickness resolution showed increased surface smoothness over 100 µm and 160 µm samples. The lower layer thickness stents contained a relatively smooth surface, where an increase in layer thickness strongly accentuated a 'step-layer' interface. Nevertheless, apart from the step-layer surface, the overall surface finish between the configurations was reasonably similar. Nonetheless, the surface roughness is still too dissimilar compared to the currently clinically used CoCr-stent (Figure 3.6 a-b), which shows a much more polished unwrinkled surface roughness.

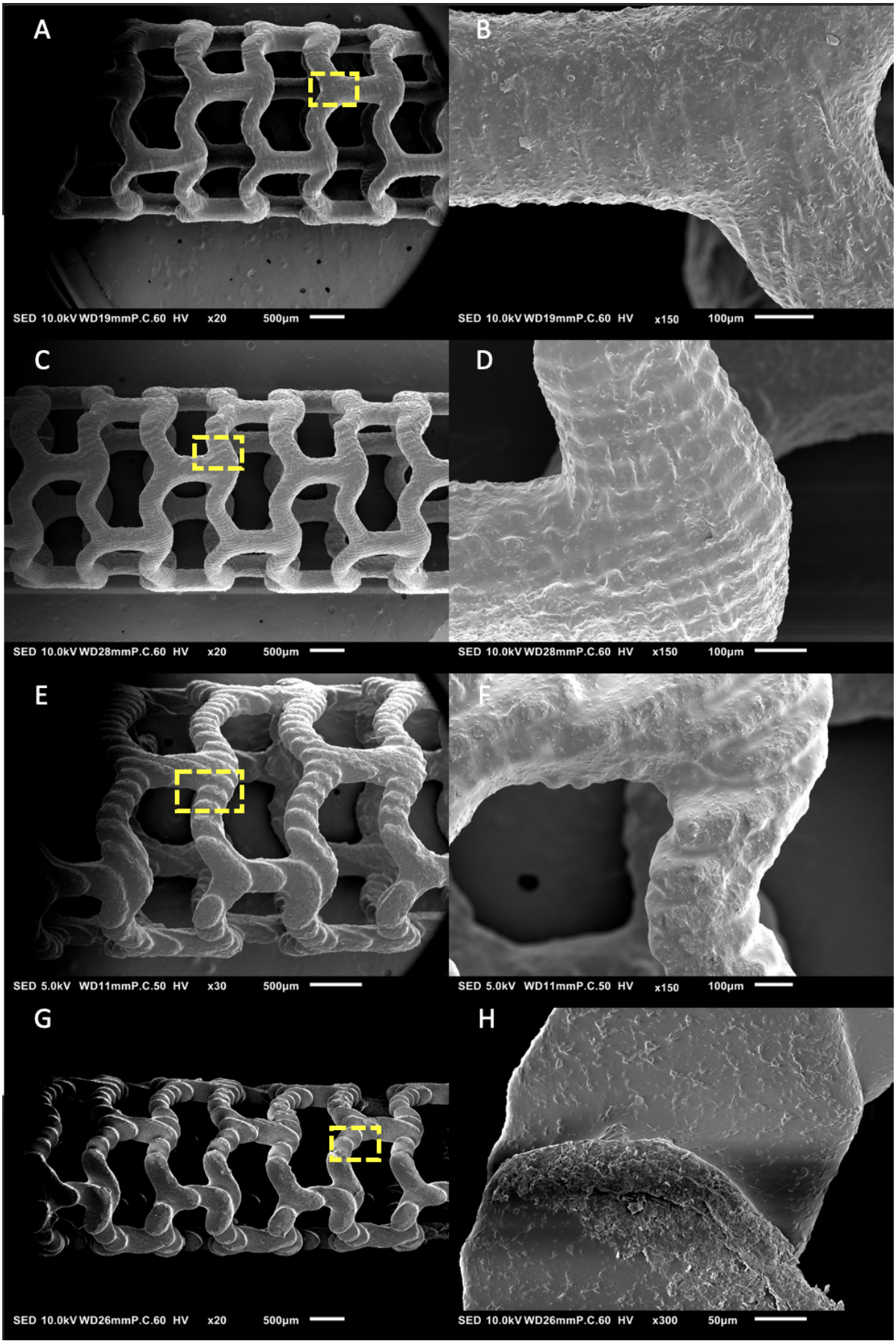

Figure 3.5: SEM images depicting the surface smoothness of non-biodegradable stents comprising the layer thickness configurations: (a-b) 25 µm-, (c-d) 50 µm-, (e-f) 100 µm-, (g-f) 160 µm. For b, d, f and h the dotted section is enlarged to 50- 100 µm depicting the porous structure. All images were obtained in the central section of the stent.

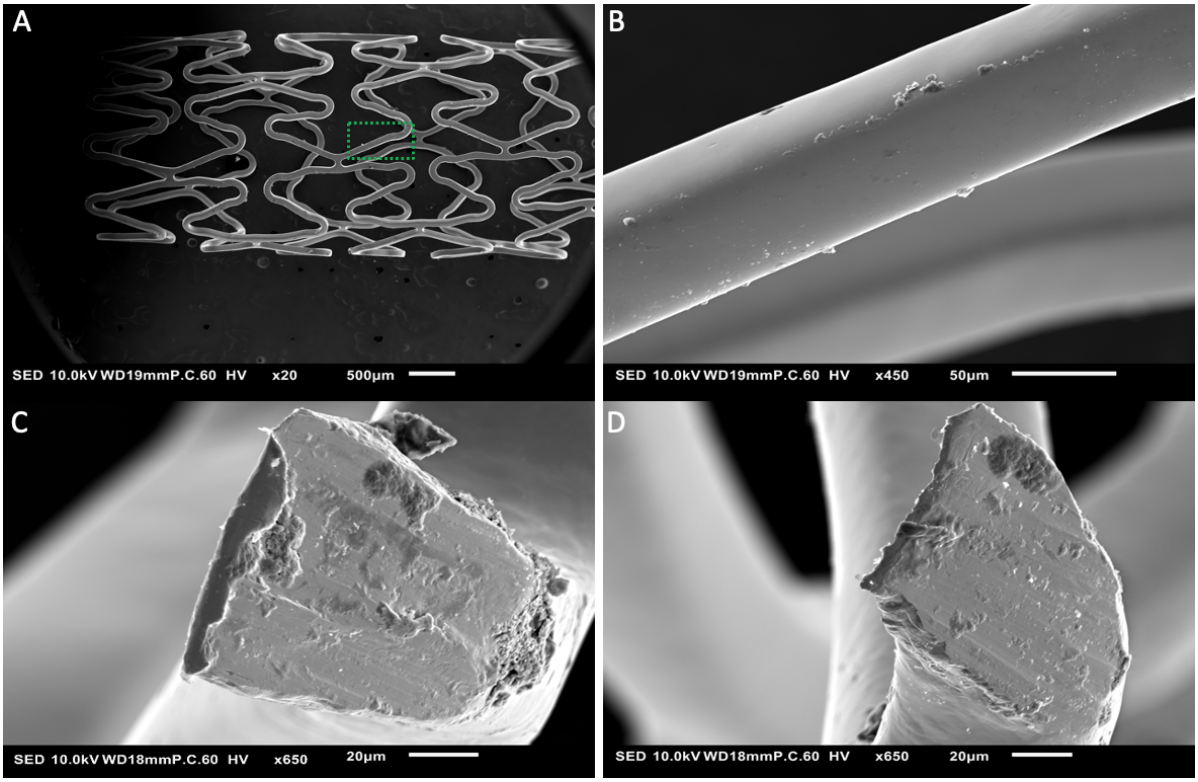

Figure 3.6: SEM images depicting (a) an overview (b) the surface smoothness (dotted section is enlarged to 50 µm), (c) a sagittal cross section and (d) a transverse cross section of a CoCr-stent (Fortimedix BV, The Netherlands).

3.2.1.2. Surface roughness

To quantify the stents' surface roughness, this particular research focuses on roughness average R_a, which is the arithmetic average of the absolute values of the roughness profile ordinates. The interferometry microscope was deployed to analyze all configurations. Figure 3.7 shows the optical images of the different configurations, whereas Figure 3.8 shows the quantification of these images. From this data, several observations can be made. First, the R_a values were approximately 600-700 nm, including a relatively large standard deviation. Secondly, the (non-parametric) Kruskal Wallis H tests showed no statistically significant difference (0.262, $p < 0.05$) between the configurations, implicating the distribution was the same across all groups. The Atomic Force Microscope was used to verify the (LT 25 µm group) Interferometer results (Figure 3.9). This indication was provided by a single measurement, suggesting no substantial dissimilarity between the two measurement methods.

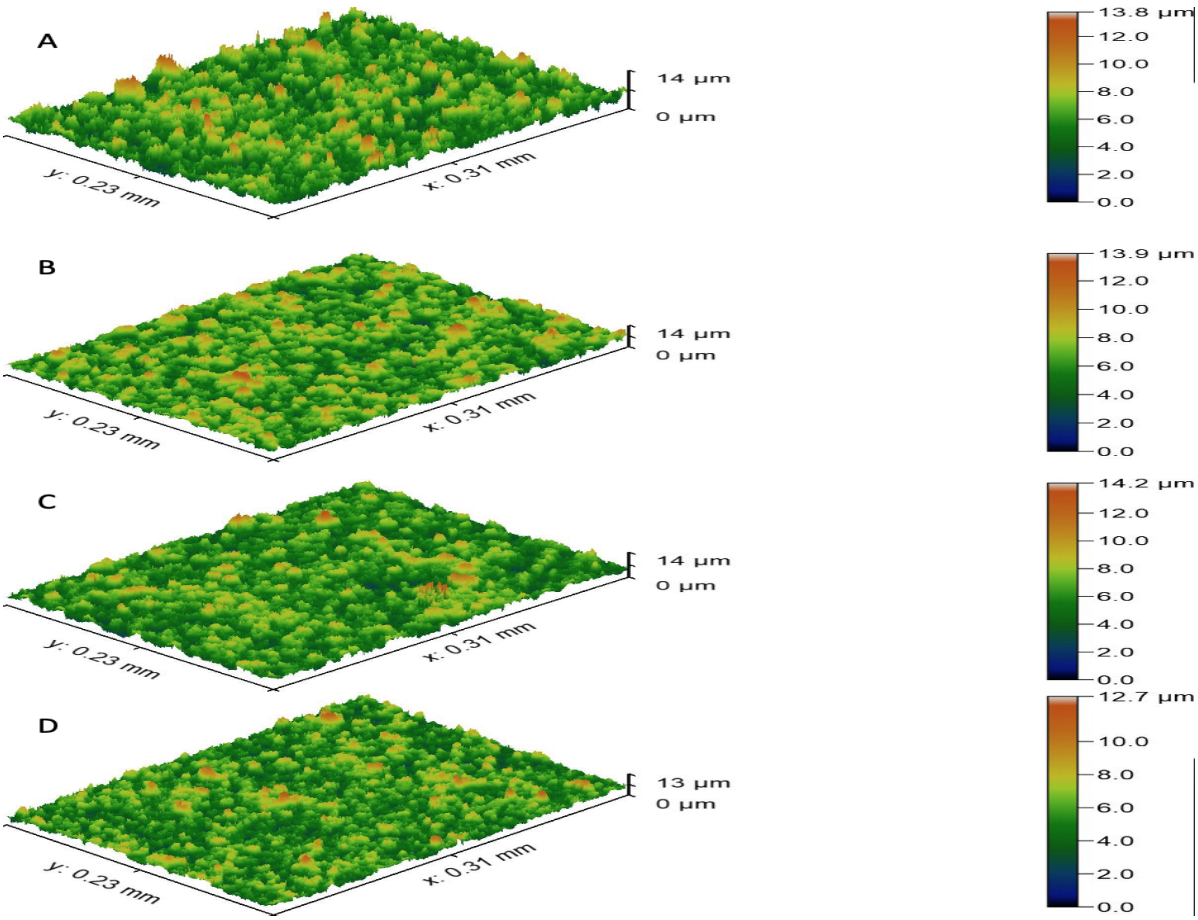

Figure 3.7: Interferometry images depicting the average surface roughness (R_a) of the non-biodegradable stents (A) LT 25 µm, (B) LT 50 µm, (C) LT 100 µm and (D) LT 160 µm.

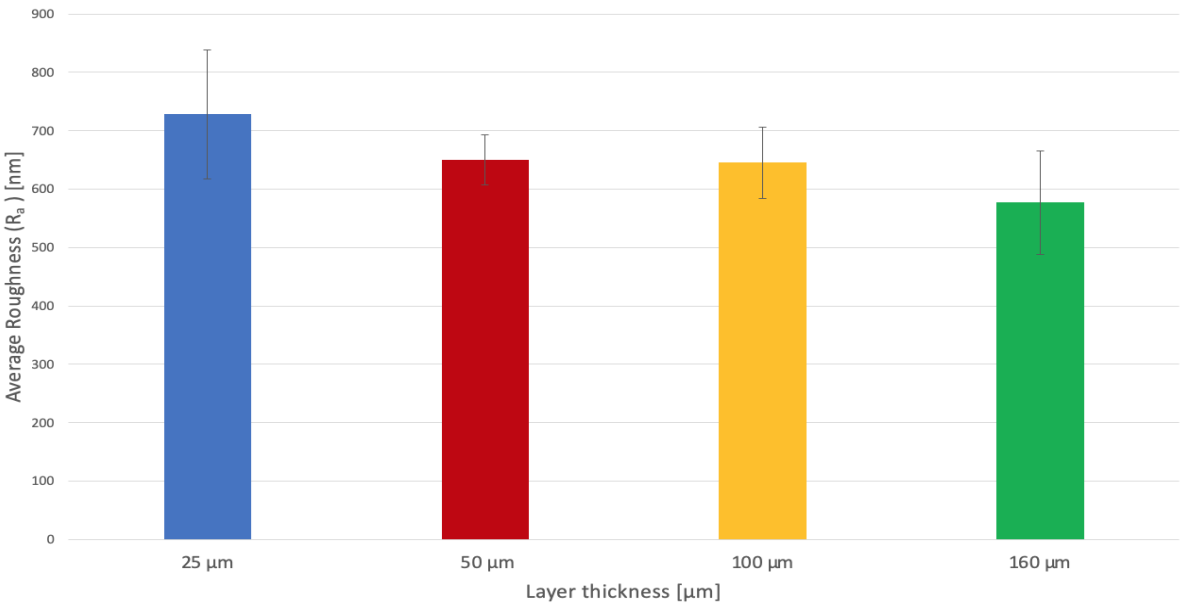

Figure 3.8: Average surface roughness (R_a) quantification measured using Interferometry. No statistical significance between the groups was perceived.

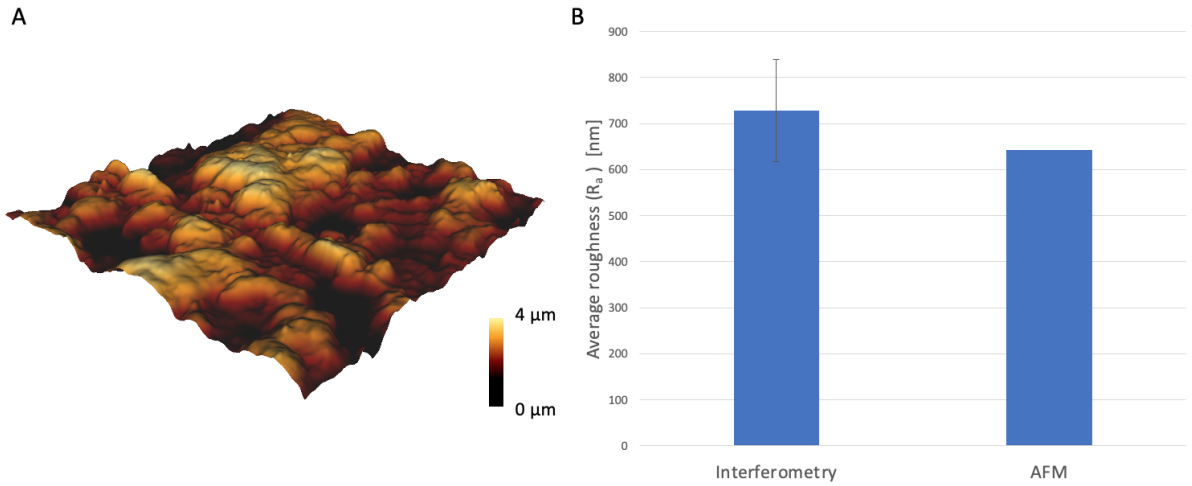

Figure 3.9: A: AFM image of the average surface roughness (R_a), B: a comparison between the AFM and Interferometry results (LT 25 µm configuration).

3.2.1.3. Fractographic analysis

The cross-section structure analysis showed similar results between layer thickness resolution as the surface analysis, endorsing the dominance of the two smaller layer thicknesses. Observation highlighted that 25- and 50 µm samples contained much greater homogeneous en dense properties than the 100 and 160 µm stents (Figure 3.10), both in the transverse and the sagittal plane. Also, the intended round structure flattened out with a decrease in layer thickness. Still, the cross-section properties are not as dense and homogeneous as the previously mentioned CoCr stent (Figure 3.6 c-d). Lastly, it is important to note that the particles present on the surface of the samples, visible in the figures, were embedded in the material itself.

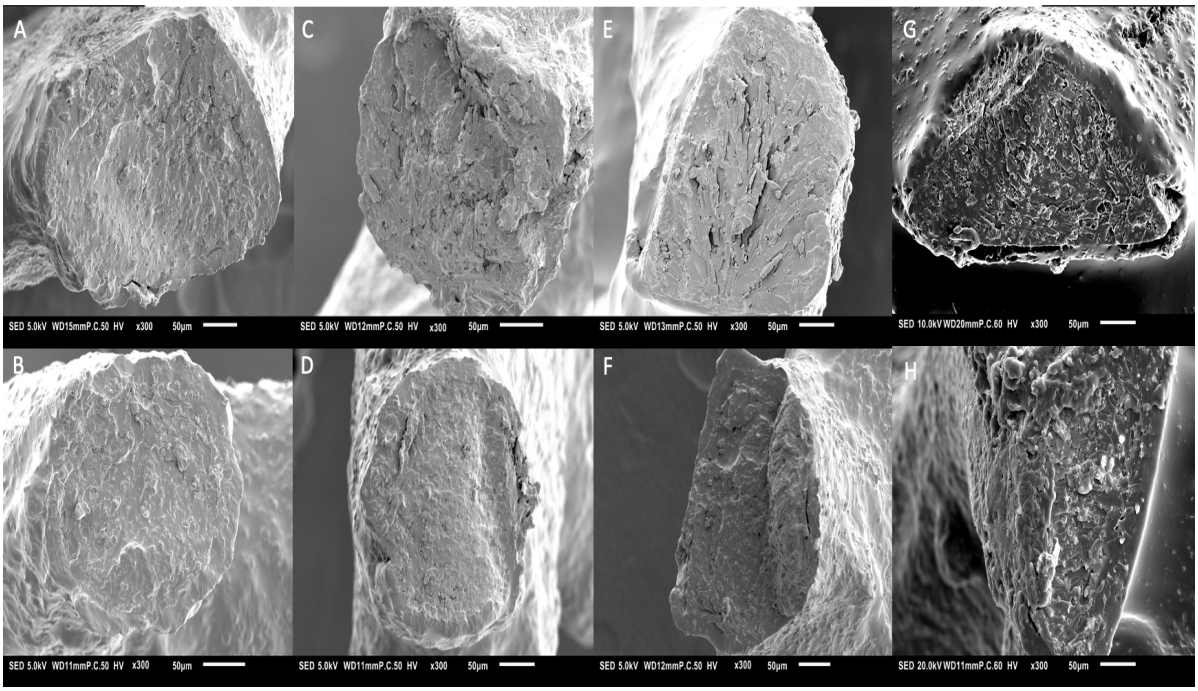

Figure 3.10: SEM images depicting the cross section structure of non-biodegradable stents (A) LT 25 µm, transverse plane, (B) LT 25 µm, sagittal plane, (C) LT 50 µm, transverse plane, (D) LT 50 µm, sagittal plane, (E) LT 100 µm, transverse plane, (F) LT 100 µm, sagittal plane, (G) LT 160 µm, transverse plane and (H) LT 160 µm, sagittal plane.

3.2.1.4. Printing accuracy

Strut thickness

Although SLA showed decent homogeneity, the measurement of the strut thickness exposed the inaccuracy of this 3D printing technique. For the non-biodegradable stents (Figure 3.11), the dissimilarity of strut thickness was the lowest (average 3.93%), and thus the most favourable, within the 25 µm layer thickness stents. This result was followed by 11.64%, 15.56% and 49.74% from the 50 µm, 100 µm and 160 µm stents, respectively. Additionally, the standard deviation showed similar high-value outcomes with 12.94%, 13.43%, 16.91% and 9.39% for respectively the 25 µm, 50 µm, 100 µm and 160 µm layer thickness stents. These outcomes sustain the non-homogenous characteristics of these non-biodegradable fabricated stents. Furthermore, the Kolmogorov-Smirnov test of normality endorsed that the data set does not fit into a Gaussian distribution, and so a (non-parametric) Kruskal Wallis H tests were performed. Last mentioned presented a significance of 0.00, $p < 0.05$, indicating a statistical difference between the LT 25, 50 and 100 µm configurations and the LT 160 µm group. However, no statistical significant difference was observed between LT 25 µm and LT 50 µm, LT 100 µm, 0.162 and 0.060, $p < 0.05$, respectively and LT 50 µm and LT 100 µm, 0.654, $p < 0.05$. The Bonferroni correction for multiple tests has adjusted significance values.

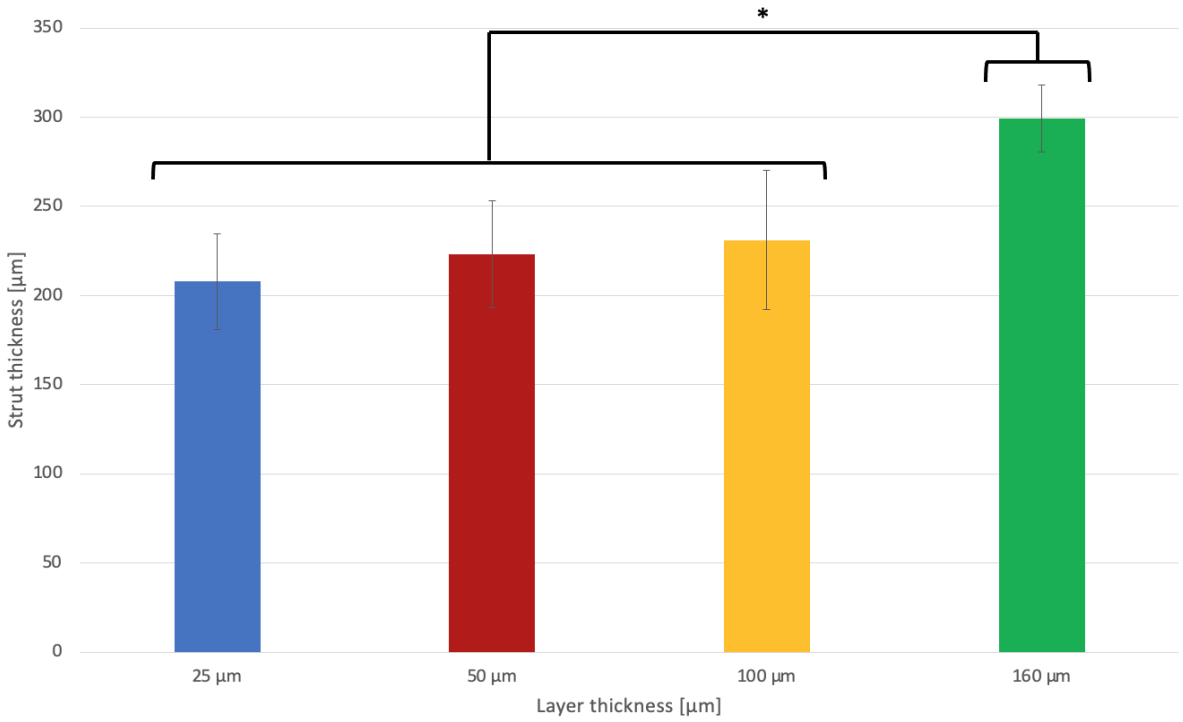

Figure 3.11: Accuracy measurements of non-biodegradable stents on the strut thickness, involving ten (200 µm) stents per layer thickness that were measured. Statistical significance with $p < 0.05$ (*) is presented between the 160 µm group and the remainder configurations.

Outer diameter

The non-biodegradable stents showed high accuracy regarding outer diameter (Figure 3.12). The specific layer thickness resolution does not seem to influence the diameters' accuracy. The measured diameters were all in a range of 92.3% (160 µm) to 98.0% (100 µm) correspondence to the intended 3 mm outer diameter stents, with a standard deviation of 0.57%, 0.85%, 1.36% and 1.67% for the 25 µm, 50 µm, 100 µm and 160 µm layer thickness stents, respectively. The number of measurements was increased from 1 measurement per sample (10 samples per group) to 3 measurements per sample (10 samples per group) in order to prevent low variance and analyze the intra user dependency because measurements were performed by hand and not automatic. The Shapiro Wilk test of normality endorsed that the data set does not fit into a Gaussian distribution, and so a (non-parametric) Kruskal Wallis H tests were performed. The latter showed no statistical difference between the various layer thickness resolutions displaying a significance of 0.073, $p > 0.05$.

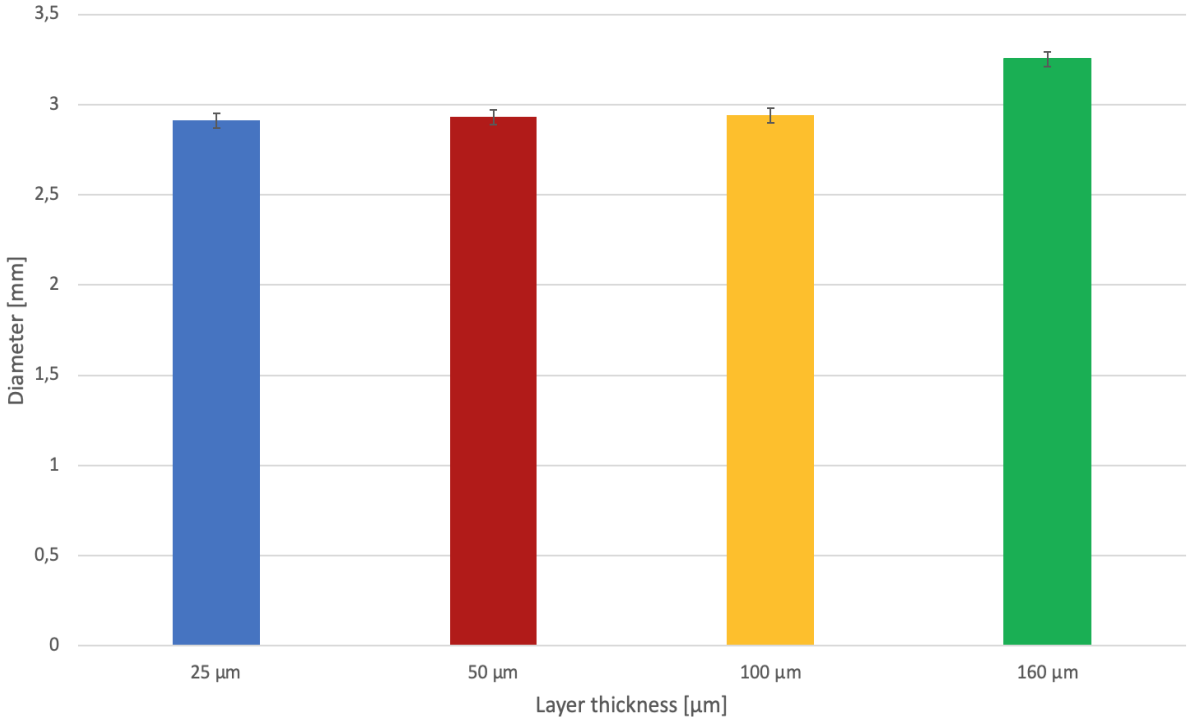

Figure 3.12: Accuracy measurements of non-biodegradable stents on outer diameter, involving ten (3 mm) stents per layer thickness that were measured. No statistical significance between the groups was observed.

3.2.2. Mechanical properties

3.2.2.1. Effects of post-processing times on stent radial strength

First, to raise conversion and improve the mechanical properties of the model, the effect of post-processing times on the mechanical properties of all configurations was investigated. A stent's primary and initial function is to support the dilated vessel and prevent (partial) prolapse of tissue. In this context, the ability of the stents to endure the loading force from the lesioned vessel, radial compression tests were performed. The non-biodegradable stents were analyzed qualitatively using trend lines to practically evaluate when to stop with the post-processing routine. Figure 3.13 shows that increased post-processing times enhance radial strength in all configurations; however, only up until 45 min of exposure time (UV exposure). After this period, a decreased radial strength is observed, implicating no eminent benefit for longer post-processing times. Consequently, 45 min was set as 'norm' for all supplementary mechanical analysis. It is important to note that to pursue the ultimate goal of creating fast on-the-spot and on-demand printing of patient-specific cardiovascular stents, the fabrication times needed to be as short as possible. Secondly, according to the literature [39][60], the stents should resist at least a load of circa 1N when 25% radially compressed, meaning it should keep blood vessels open after angioplasty. So, concerning the radial strength variation between the different configurations, the 50 µm layer thickness stents showed remarkably higher radial strength than the LT 25, 100 and 160 µm samples (Figure 3.14). A (non-parametric) Kruskal Wallis H test was performed showing a statistically significant effect between the LT 50 µm group and both the LT 25 µm, LT 100 µm and LT 160 µm group of 0.000, $p < 0.05$. However, no statistically significant difference was found between the LT25 µm- LT 100 µm groups, 0.382, $p > 0.05$, the LT25 µm- LT 160 µm groups, 0.936, $p > 0.05$ and the LT100 µm- LT 160 µm groups 0.431, $p > 0.05$. The Bonferroni correction for multiple tests has adjusted significance values. These results endorse the suggestion that an increase in layer thickness resolution does not undoubtedly result in a higher radial strength. Three stents per measurement point were analyzed, after which the samples were cast away.

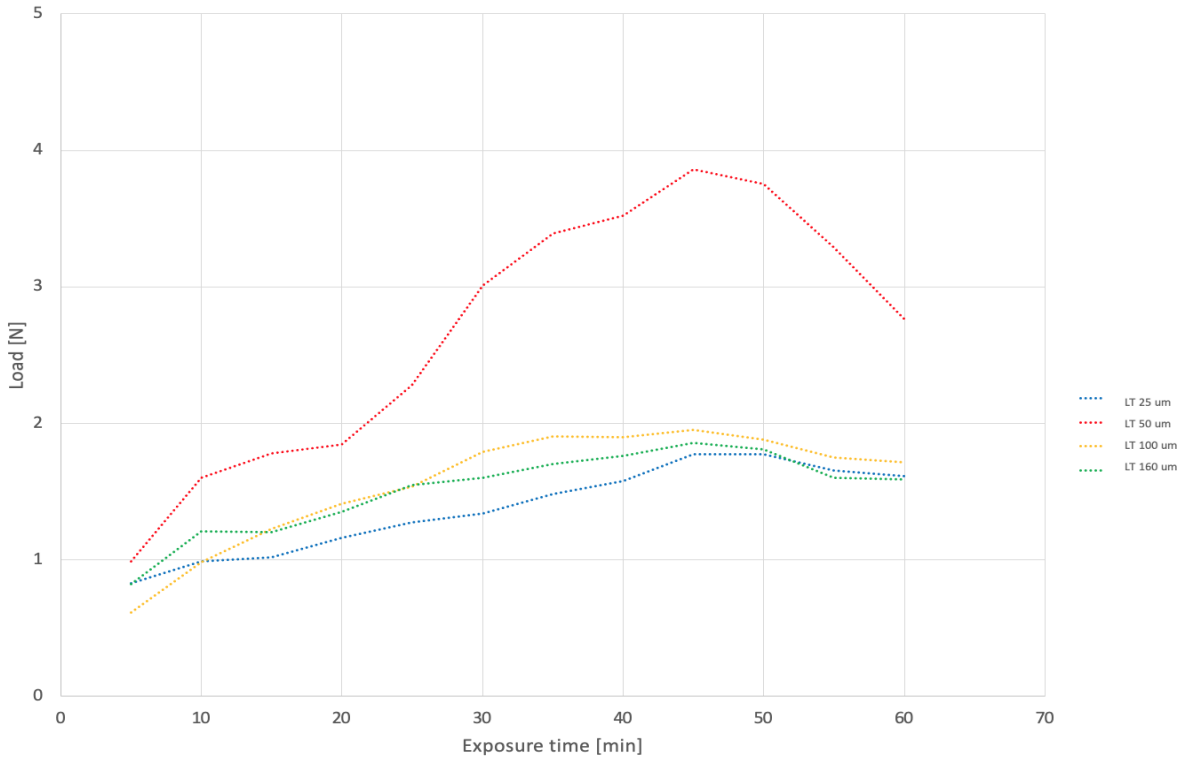

Figure 3.13: Trend lines of all configurations showing the effects of post-processing times on stent radial strength. Al groups present an increasing line up until 45 min of exposure time (UV exposure), after which it declines. Radial strength is correlated to a horizontal compression force (y-axis) and the impact of exposure time (x-axis), which indicates the post processing time (UV chamber).

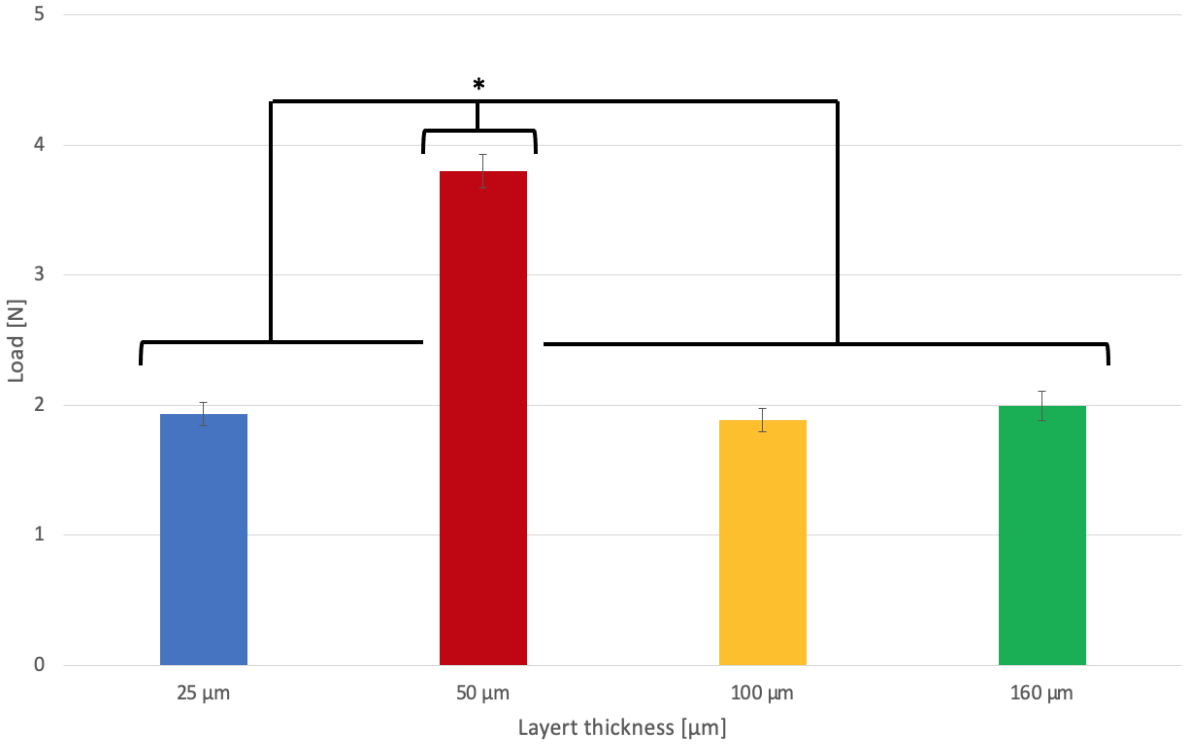

Figure 3.14: Radial strength analysis of non-biodegradable stents, up to 25% compression of the initial diameter (3 mm). Radial strength is correlated to a horizontal compression force (y-axis) and the various configurations (x-axis). The minimal required value is 1 N. Statistical significance with $p < 0.05$ (*) is presented for the non-biodegradable stents between the LT 50 µm group and the remainder groups LT 25 µm, LT 100 µm and LT 160 µm.

3.2.2.2. Viscoelastic effect

The samples were radially compressed over one cycle (load-unload) to account for potential viscoelastic effects on compression behaviour. Figure 3.15 a-d shows the compression diagrams obtained for all tested configurations at various deformation rates (0.2, 0.5, 1.00, 1.25, 1.50, 1.75, 2.25 and 2.75 mm/s). Several observations can be made. First, the load-deformation diagram for all groups follows a hysteresis loop shape at the majority of the deformation rates, indicating that energy is dissipated over the compression process. Some slight variability among the deformation rates could be identified with differences around 46% (1.50 mm/s vs 2.75 mm/s for LT25 µm) regarding the peak radial force. To this extent, the outcomes endorsed the maximum deformation rate of 1.75 mm/s, which is the equivalent of 70 bpm. Higher deformation rates (2.25 and 2.75 mm/s) showed indications of viscoelastic effects.

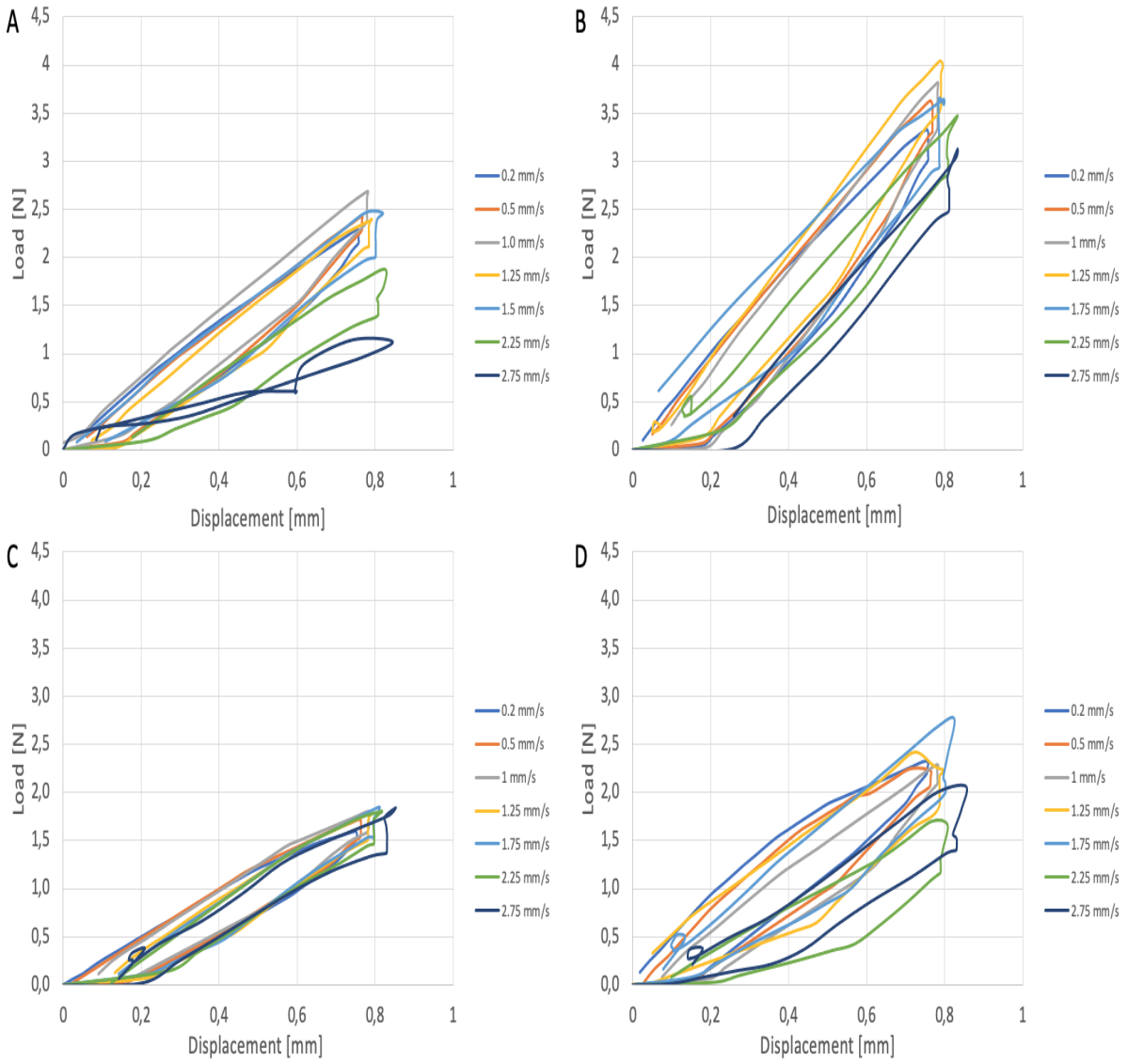

Figure 3.15: Compression diagrams obtained over 1 cycle for all tested configurations at various deformation rates (0.2, 0.5, 1.00, 1.25, 1.50, 1.75, 2.25 and 2.75 mm/s) to account for potential viscoelastic effects. Diagram A represents LT 25 µm, B: LT 50 µm, C: LT 100 µm and D: LT 160 µm.

3.2.2.3. Cyclic loading

The stents' long-term recovery potential was analyzed by applying successive cyclic radial 25% deformations at 1.75 mm/s. Up to 4200 cycles of a sinusoidal function of displacement were used to mimic pulsatile arterial pressure and defined as a dynamic loading group. The experiment involved stents placed horizontally in a compression machine (Instron Electropuls E10000, Instron, USA) exploiting a 10 kN load cell. Although the resistance load of the stents were in the noise range of the compression machine, Figure 3.16 clearly shows the differences between the Maximum and Minimum load, where the blue line (Maximum) corresponds to 0% compression and the orange line (Minimum) to 25%. If these parameters were be displayed as parallel lines, no mutations in the design structure are expected, as shown in Figure 3.16-a (LT 25 µm). The remainder configurations showed interruptions and narrowing of the Maximum and Minimum load, thus predicting fracture in the samples. Figure 3.17 endorsed the last-mentioned findings and demonstrates the rupture of the LT 50 µm, LT 100 µm and LT 160 µm. Subsequently, the number of cycles was increased to 67200 cycles for only the LT 25 µm samples. The latter, as the other configurations, already showed fractures at 4200 cycles. Figure 3.18-a shows a re-narrowing of the Maximum and Minimum load at approximately 63000 cycles, a matter which is endorsed by Figure 3.18-b.

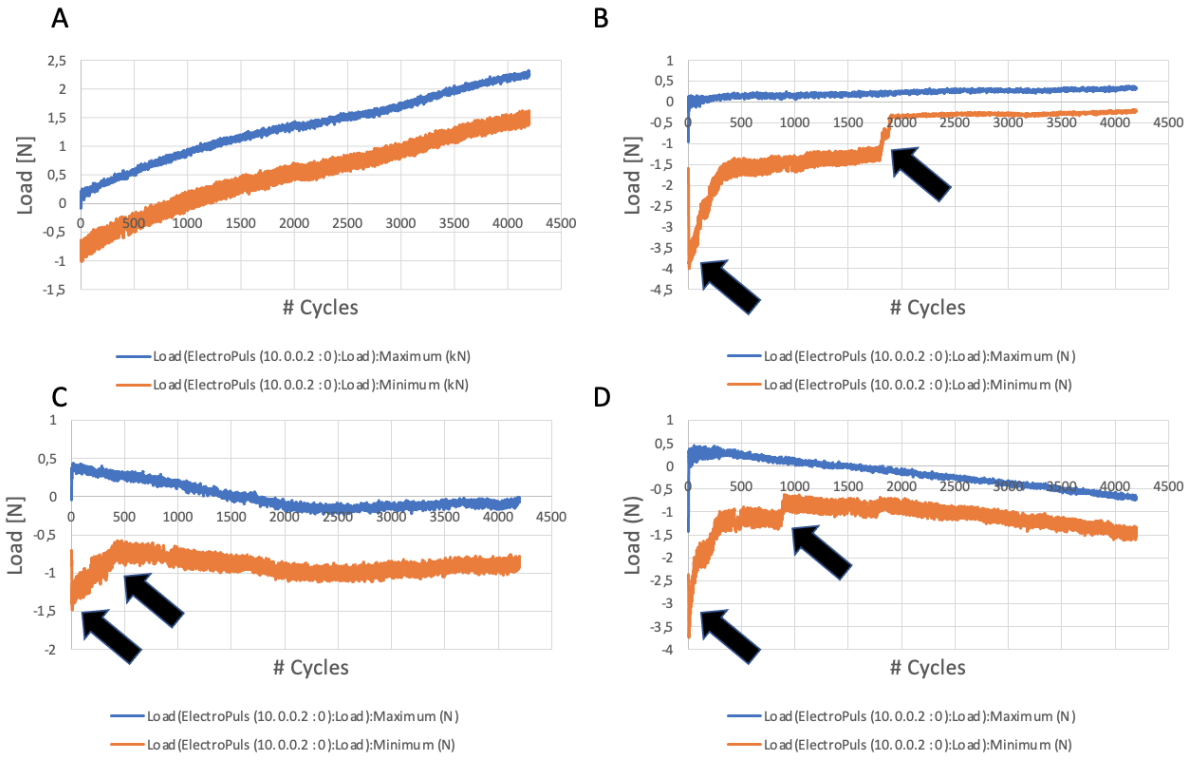

Figure 3.16: Cyclic compression (25%) of all configurations (A: LT 25 µm, B: LT 50 µm, C: LT 100 µm and D: LT160 µm) up to 4200 cycles. The absolute values are not applicable, yet the diagrams clearly show the differences between the Maximum and Minimum load (blue line (Maximum) corresponds to 0% compression and the orange line (Minimum) to 25%. If interruptions and narrowing of these parameters occur (arrows), mutations in the design structure and fracture in the samples is predicted. The consequence of these alterations are shown in Figure 3.16.

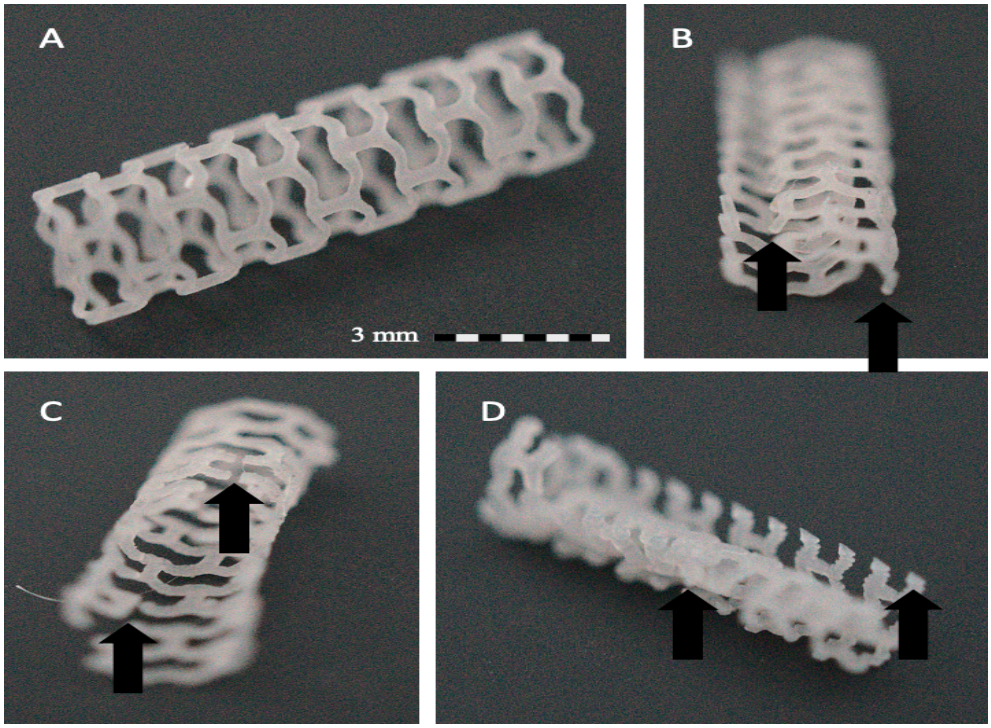

Figure 3.17: Images of the samples (A: LT 25 µm, B: LT 50 µm, C: LT 100 µm and D: LT160 µm) after 4200 cycles of cyclic compression (25%). The arrows demonstrate fractures that emerged from the alteration of the Maximum and Minimum load values demonstrated in Figure 3.16. The scale bar presented in A is similar for B, C and D.

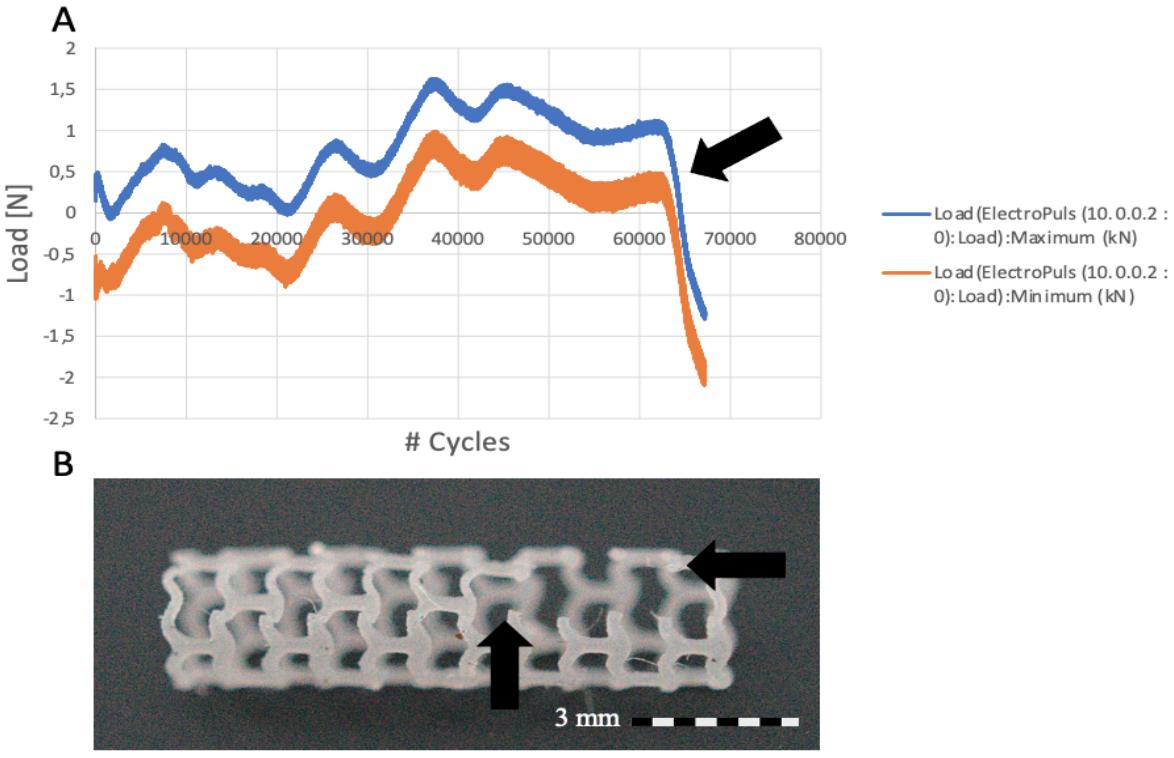

Figure 3.18: Composed figure obtained from cyclic compression loading (63000 cycles) on LT 25 µm configuration, showing A: diagram presenting the Maximum and Minimum load and B: sample after the analysis. The arrows demonstrated the interruptions and narrowing of the presented parameters (A), involving the consequences of the alterations (fractures) (B).

3.2.2.4. Tensile tests

Tensile testing of the non-biodegradable material was performed to identify the strength of the different configurations under the action of the tensile loading's. Several parameters were investigated. First, a SolidWorks simulation was deployed to determine if the load distribution within the customized tensile bar was accurate (Appendix C). Stress and strain behaviours of the prepared samples were used to calculate the Young's Modulus (YM) (Figure 3.19) and the Ultimate Tensile Strength (UTS)(Figure 3.20). The Young's Modulus is generally defined as material stiffness, and thus it is material dependent. As shown in Figure 3.19, the average Young's Modulus is circa 233.64 MPa, and the (non-parametric) Kruskal Wallis H tests showed no statistically significant difference between the configurations (0,367, $p < 0.05$). Figure 3.20 evidently shows that an increase in layer thickness does not necessarily cause enhanced Ultimate Tensile (or breaking) Strength values. The (non-parametric) Kruskal Wallis H tests showed a significance of 0.015 and 0.001, $p < 0.05$, indicating a statistical difference between the LT 25 µm, LT 50 µm categories and the LT 160 µm group. However, no statistical significant difference was observed between LT 25 µm and LT 50 µm, 0.365, $p < 0.05$, and LT 100 µm and LT 25 µm, LT 50 µm and LT 160 µm, 0.373, 0.074 and 0.127, $p < 0.05$. The Bonferroni correction for multiple tests has adjusted significance values.

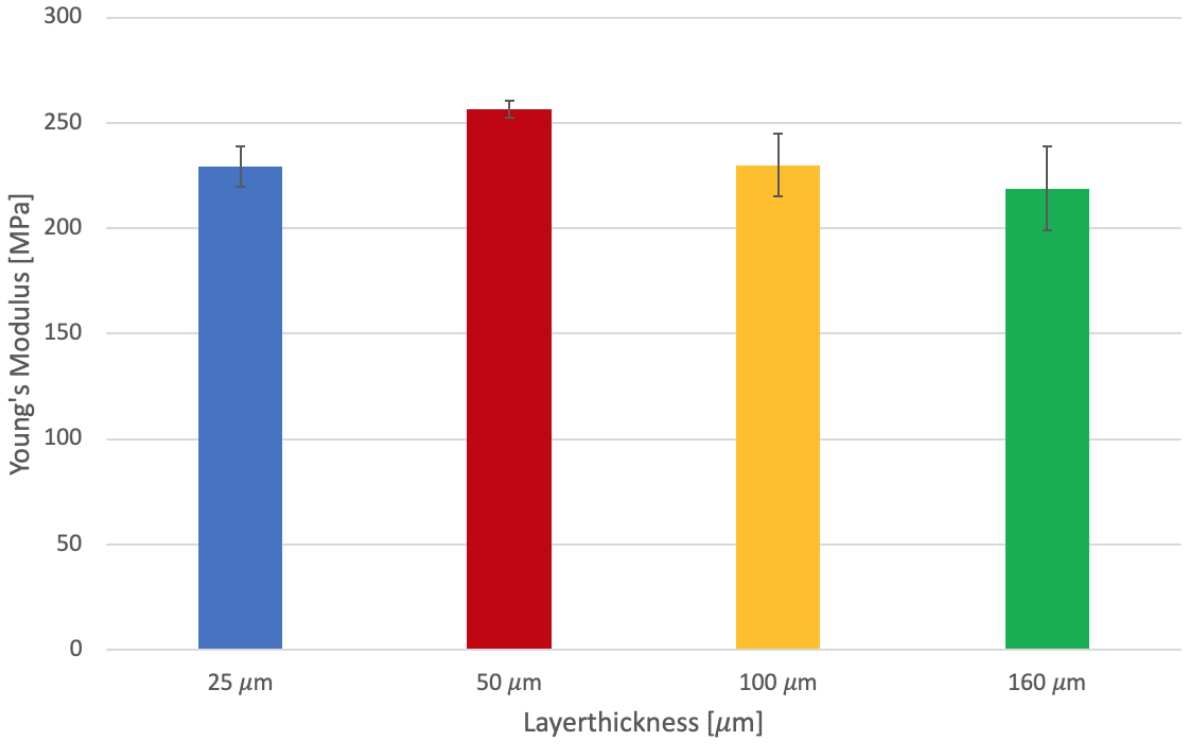

Figure 3.19: Young's Modulus of all configurations of the non-biodegradable stents, involving similar material. No statistical significance was observed.

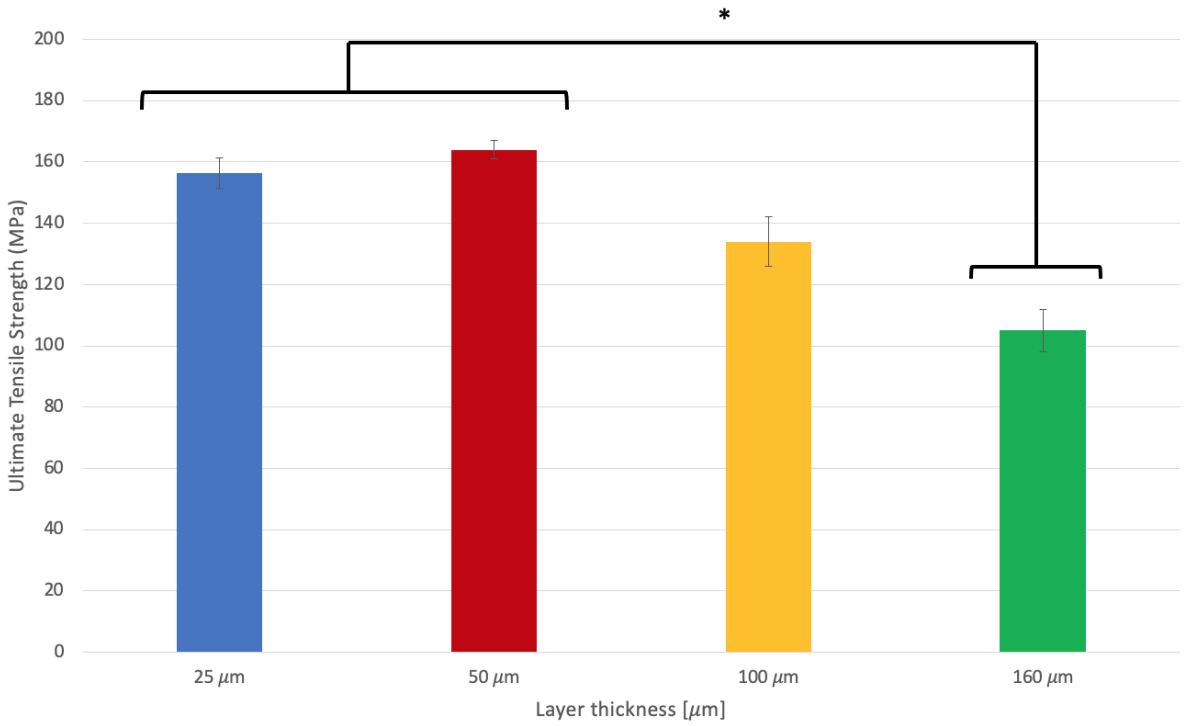

Figure 3.20: UTS analysis of non-biodegradable stents, up to failure. Statistical significance with $p < 0.05$ (*) is presented for the non-biodegradable stents between the LT 25, 50 µm groups and the LT 160 µm group.

3.2.2.5. Longitudinal compression

With a compression force of 0.5 N, the stents with the least longitudinal integrity shortened the most, and those with the greatest longitudinal integrity compressed the least. Similar to the radial strength results of the non-biodegradable stents, the LT 50 µm group showed a smaller percentage of distortion (1.48%) compared to the LT 25, 100 and 160 µm configurations 1.95%, 2.10% and 2.14%, respectively (Figure 3.21). However, the (non-parametric) Kruskal Wallis H tests showed a significance of 0.016, $p < 0.05$, indicating only a statistical difference between the LT 50 µm and the LT 160 µm groups (0.018, $p < 0.05$). The Bonferroni correction for multiple tests has adjusted significance values. To put these results in perspective, the two most commonly used stents worldwide [61], the Xience (Abbot, USA) and the Promus Element (Boston Scientific, USA)) showed much greater displacement factors of 3.57% and 17.86%, respectively. These longitudinal deformation outcomes highlight the essential role of connectors regarding longitudinal integrity since distortion is heavily linked to the number of connectors. The non-biodegradable stents contain four connectors, while the Xience and Promus Element consist of 3 and 4, respectively. The hoops of the stent provide support, while the connectors hold the hoops together and thus prevent longitudinal distortion. However, increasing the number of connectors lowers the flexibility of the stent, which is unfavourable for the delivery process.

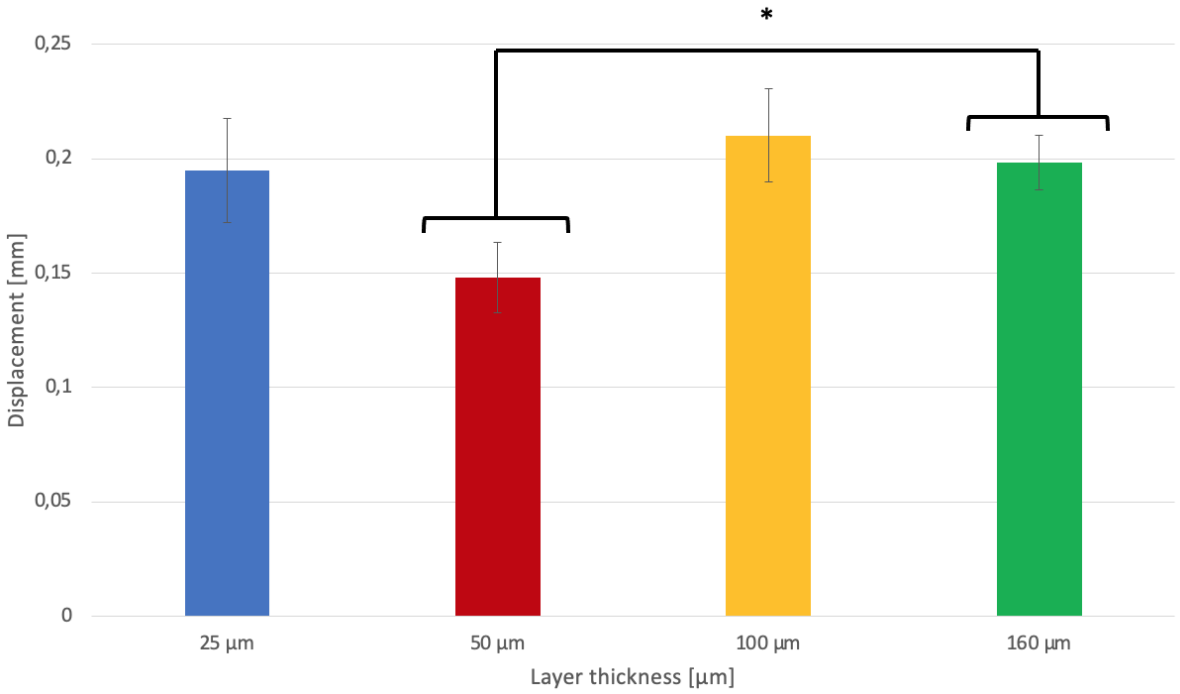

Figure 3.21: Longitudinal deformation of non-biodegradable stents, up to 0.5 N vertical compression force. Although the LT 50 µm configuration appears to outperform the remainder configurations, no statistical significant difference was found.

3.2.3. Resin viscosity

The viscosity of a resin is a vital point in the effective printing of samples. Figure 3.22 shows the diagrams obtained for both the biodegradable resin and the non-biodegradable resin. Various observations can be made. First, the non-biodegradable resin involves the commercial resin, indicating an optimal viscosity for the deployed SLA printer and corresponding settings. Secondly, the biodegradable resin showed a substantially higher viscosity average of 2.72 x 10x4 mPa.s, compared to the commercial resin (average 1628 mPa.s).

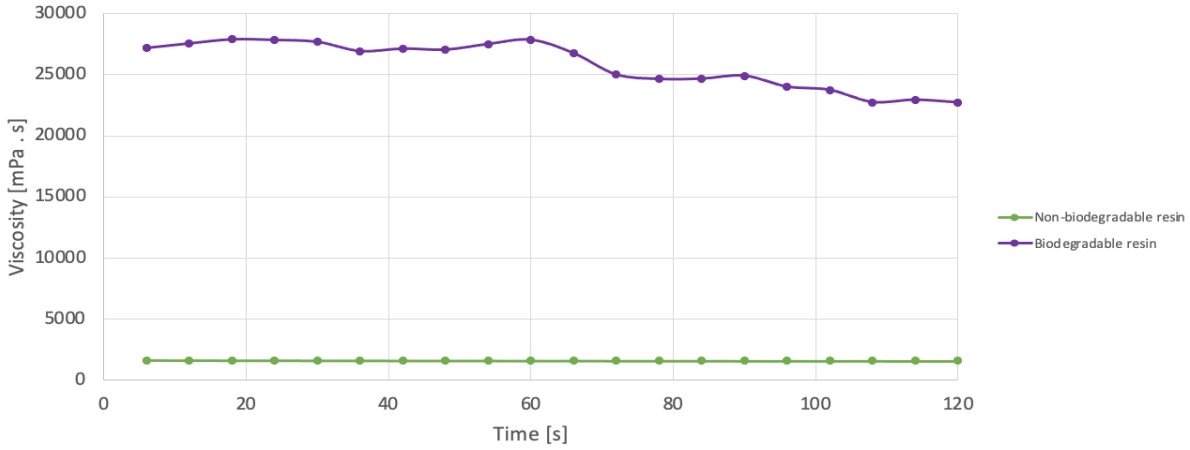

Figure 3.22: Viscosity measurements for the non-biodegradable resin (AVG 1628 mPa.s) and the biodegradable resin (AVG 2.72 x 10x4 mPa.s).

4

Discussion

Since the introduction of the first bare metal stent (BMS), vascular stents have improved in multiple aspects. BRS are considered state of the art, but still, no bioresorbable stent is currently commercially available. Besides, (bioresorbable) stents are not able to adhere to patient-specific needs. Additive manufacturing technologies, which have gained enormous traction the past couple of years, provides a potential method to respond to this increasing request for patient-specific medical implants [62][63]. This study aimed to investigate the possibilities to 3D-print a polymeric cardiovascular bioresorbable stent prepared by stereolithography that offers adequate morphology and mechanical properties for clinical applications. This aim was set to contribute to the ultimate goal of using the SLA additive manufacturing process to 3D fabricate on-the-spot and on-demand patient-specific bioresorbable stents. Moreover, it highlights the obstacles and minimal standards on printer-specific parameters, dimensions, morphological and mechanical properties to develop next-generation BRS manufactured on-site. In this research, two different (bio)materials were explored. The non-biodegradable resin (Form 3, Formlabs, USA) contained optimized printing settings and was thus deployed to investigate the limitations of the printing capabilities regarding dimensions, layer thickness, and subsequently the effect of these parameters on the morphological and mechanical characteristics. Ultimately, this variant was able to produce a stent with a diameter of 3 mm. The B-ink resin was synthesized according to the protocol of van Lith et al. [39] but did not contain the suitable characteristics concerning its viscosity, to be able to initiate a 3D printing process.

Since the 3D printing of bioscaffolds still is in its pioneer stage and resin composition characteristics, such as viscosity, acquire a precise norm and crucial role in the success rate of a print, a commercial device (Form 3, Formlabs, USA) was used to explore the limitations of SLA printing regarding dimensions and support material, using their non-biodegradable Grey Resin V4 1L (Formlabs, USA). Familiarizing and finetuning the SLA printing technique has led to novel insights concerning the limitations regarding dimensions, support structure and printing direction. Additionally, corresponding process parameters of the SLA method have a significant effect on the minimization of the previously mentioned shortcomings. Hence, it is essential to understand how process parameters affect the morphological and mechanical characteristics of models. The printing layer thickness is identified as the most influential process parameter and will be investigated in this research. Still, the main constraint that hampers the successful implementation of SLA in the biomedical sector is the limited biopolymers available. Though, recent studies [64][65][66][54] have demonstrated the development of biocompatible and/or biodegradable resins, current material offer is still limited.

4.1. Optimization SLA as manufacturing technique

As to the limitations regarding dimensions, support structure and printing direction, the research focused on 3 mm diameter cardiovascular stents. The latter because this specific dimension was set as the golden standard for mechanical testing of cardiovascular stents. This study showed that with a decrease in printing layer thickness, smaller scaffolds could be manufactured. The Form 3 is limited by its minimum layer thickness of 25 µm, but research already showed the possibility of decreasing the printing layer thickness to 5 µm [35]. Last mentioned, implicating a corresponding decrease in available dimensions. Ultimately, it should be

feasible to print considerably smaller stents, which is of great importance not only for the range of printable dimensions but also for the available strut thicknesses. These struts play an important role since the loss of radial strength using polymers, compared to existing metallic stents, needs to be compensated and thus requires bigger strut thickness. However, thicker struts hinder the healing process by prolonged biodegradation, perturb blood flow dynamics, increased shear stress and impaired reendothelialization leading to increased thrombogenicity. Secondly, the fabrication process using SLA requires added support for printing spread structures and sufficient adhesion to the printing bed. The removal of these support structures proved to be challenging, as the stents are relatively fragile. Moreover, the remains of the support material were observed at the attachment's areas (Appendix F), and thus the touchpoint size was maintained as small as permissible. In addition, if external supports cannot be avoided and are required due to the selected fabrication method, initiate the supports in a region that is not in contact with tissue. On the one hand, this will enhance a smoother surface finish which is crucial for the attachment of the stent to the tunica intima, but on the other hand, this will complicate the removal of such structures. Thirdly, the role of the printing direction varies per specific SLA technique. The layer-by-layer method (e.g. Form 3) endorsed to maintain the length to be in the printing direction. That still means each individual layer is uniformly cross-linked (in relation to the radius). Fracture could more easily come during axial flexing, but radially the stent will be more robust against vessel loads. If printed in another direction, the inverse would more likely be true. The stent would be robust against axial flexing, but the radial loading could be subjected to mechanical non-uniformity. For the 'continuous' fabrication method (e.g. Prusa SL1), the difference in mechanical properties is fairly nil. Thus, the length of the stent can be in the printing direction, and so, a print can be fabricated with the radius being perpendicular to the Z-axis. However, that would limit the total length of the stent that can be printed (projection area limited). A decisive supplementary effect of a 'continuous' fabrication method can be the elimination of the previously mentioned remaining support material issue.

4.2. Mechanical analysis

Concerning the mechanical analysis, radial strength, viscoelastic effect, cyclic loading, tensile tests and longitudinal compression were selected as corresponding tests. Primarily, radial strength because the main and initial function of a stent is to support the dilated vessel and prevent (partial) prolapse of tissue. Radial strength is mainly determined by the selected polymer, stent architecture and strut thickness. In this context, to investigate the ability of the stents to endure the loading force from the lesioned vessel and to measure for crush resistance of stents, compression tests were performed [56]. However, there is no straight answer of what value radial compression resistance is sufficient. Ware et al. [39] tested the mechanical performance of a BMS. This expanded stent showed a 1.03 N load at 25% radial compression. Subsequently, this value has been set as a minimum required value on radial strength. Besides, the Absorb GT1 (Abbott, USA) and the Xience (Abbott, USA) have a radial strength of approximately 3 N and 3.5 N, respectively (at 24 months implantation [14]. The majority of the non-biodegradable stents exceeded the minimal standard of 1 N radial strength. It should be highlighted that this study strove to meet the design and dimensions of the Absorb GT1 (Abbott, USA), and subsequently, the strut thickness (150 µm) of this particular stent was mimicked. However, due to an insufficient number of available configurations, the strut thickness was increased to 200 µm. Last mentioned, provided the ability to add multiple configurations, which was essential for investigating the effect of layer thickness. Notably, the LT 50 µm showed much greater radial strength values than the LT 25, 100 and 160 µm stents, contrary to previous research [67][68], which indicates that radial strength decreases with the increase in layer thickness. Logically, last-mentioned can be contingent; however, thinner layers also mean more time, artefacts and errors. To be more specific, thinner layers coincide with additional repetitions (longer printing times) and, thus, greater opportunities for something to go wrong. For example, even at a 99.99% success rate per layer, quadrupling the resolution lowers the chance of print success from 90% to 67% if one assumes that a failed layer causes a total print failure. In fact, according to the company behind the Form 3 SLA printer, printing models at lower resolutions (i.e. thicker layer heights) can result in higher-quality prints. Hence, high resolution comes with a trade-off. Furthermore, due to stresses or mechanical loading, implants can form micro-cracks, resulting in increased surface exposure to water and a faster degradation process [121]. Subsequently, the radial strength of the hoops has a great impact on the degradation process of the biomaterials as well [69]. Ensuing, the effect of post-processing on radial strength was analyzed, resulting in roughly increased radial strength over time until 45 min. From this time mark, there was a slight decrease in radial strength. Post-processing generally consists of a solvent used to remove unreacted

monomer followed by UV exposure, all employed to raise conversion and improve the mechanical properties of the model [70]. The former can either be employed by a quick solvent 'rinse' to remove monomers on the surface or a longer 'soak' to remove monomer from the model's interior. Additionally, due to the high absorber concentration, a 'candy-shell' effect occurs, where only a thin layer on the outside of the model is hardened. So, a thermal or UV post-cure is suggested to achieve a higher conversion value in the entirety of the model, not limited by photo-absorber [71]. However, both adjustments will increase the manufacturing time drastically [35][71].

With the radial strength and optimal post-processing time determined, it was interesting to analyze the effect of cyclic loading to expose potential fatigue characteristics on the different layer thickness configurations. As the FDA strongly recommends testing the cardiovascular stents for 10- 15 years *in vivo* concerning cyclic loading (400- 600 million cycles) [72], the deformation rate must be considerably high to lower the experimental running time. The non-biodegradable stents were first radially compressed over one cycle (load-unload) over a 25% radial deformation to account for potential viscoelastic effects on the compression behaviour. The test was performed at multiple deformation rates 0.2, 0.5, 1.00, 1.25, 1.50, 1.75, 2.25 and 2.75 mm/s, corresponding to 8, 20, 40, 50, 70, 90, 110 beats/min heart rate respectively. The outcomes showed a load-deformation diagram that follows a hysteresis loop shape at most deformation rates, indicating that energy is dissipated over the compression process. Some substantial variability among the deformation rates could be identified with differences around 46% (1.50 mm/s vs 2.75 mm/s for LT25 µm) regarding the peak radial force. To this extent, the outcomes endorsed the maximum deformation rate of 1.75 mm/s, which is the equivalent of 70 bpm. Secondly, the stents' long-term recovery potential was then evaluated by applying successive cyclic radial 25% deformations (from 4200 up to 67200 cycles) at a 1.75 mm/s deformation rate. Preferably, a fatigue test would involve *in vivo* circumstances and biaxial loading, mimicking an artery as adequate as possible. Unfortunately, no similar or comparable equipment was available at the TU Delft, and thus, a linear all-electric dynamic machine was deployed. The Instron Electropuls E10000 fatigue bench press simulated a sinusoidal function of displacement to mimic pulsatile arterial pressure. However, the compression was uniaxially distributed and centred at a point stress area. Also, the resistance load of the stents were in the noise range of the machine, and thus no absolute values could be obtained; only relative data could be extracted, implicating the analysis is more to a visibility study. The Instron Electropuls E10000 precision goes down to 1/250 of the load cell full scale, indicating an accuracy of 40 N. Hence, a 100 N load cell is recommended to increase the accuracy scale and prevent the observed excessive drift. The sine wave was adequately simulated, and the measured load pursues the sine wave accurately. The Maximum and Minimum load were displayed as parallel lines; only due to a large drift both lines move up during the experiment. Alterations between the parameters indicate fracture(s) of the samples. The results endorsed the above-mentioned suggestion, supported by the images (Figure 3.16). All configurations, except for the LT 25 µm, did show fracture after 4200 cycles. Subsequently, the number of cycles was increased (LT 25 µm solely) to 67200 cycles to investigate the fatigue behaviours in-depth. As presented in Figure 3.17a, after approximately 63000 cycles, the stent showed several fractures endorsed by the image (Figure 3.17b). It is important to note that a single or even multiple mutations (s) in these graphs indicate a fracture in the stent; however, this does not necessarily imply a total failure of the construct. For example, as demonstrated in Figure 3.18, several struts have indeed failed, but the construct as a whole is still resistant to a particular radial strength.

The deliverability of the stent is an essential factor for the success rate of the whole stenting procedure. A cylindrical tensile bar comprising a stent in the middle section was developed to examine the flexibility and its ability to withstand tensile strength. The YM and UTS of the stent were determined by uniaxial tensile testing. A SolidWorks simulation showed ideal load distribution among the tensile bar, implicating a maximum load in the middle of the bar/stent. The Elastic Modulus, or so-called Young's Modulus, is a mechanical property that measures the tensile stiffness of solid material, or the distance between the molecules and the bond strength in between, to be more specific. It quantifies the relationship between tensile stress and axial strain in the linear elastic region of a material and thus should be similar for all configurations since the non-biodegradable material is similar among the configurations. However, the non-biodegradable stents fabricated for the needs of this thesis are not moulded, but additive manufactured, indicating a layer-by-layer mechanism. The latter inevitably implies the formation of a laminated structure. Besides, the stent within the tensile bar adds another shape component, moving the focus from the elastic modulus more to the stiffness characteristics. Yet, the results did endorse the expected outcomes indicating no statistical difference. The average Young's Modulus was approximately 225 MPa, which is in the range of the minimal mechanical re-

quired 200 MPa [73]. Numerous facets within the material properties can be adjusted to increase the Young's Modulus, such as increasing the carbon chain length of the polymers' part D, as described in Figure 3.3. Last mentioned approach can be used to generate a more flexible stent that is easier to manoeuvre through the arteries to the ultimate lesion site. Furthermore, the UTS results showed a dominance of the LT 25 and 50 µm groups over the remainder configurations (LT 100 and 160 µm). All obtained values are not within the set requirements, stating a minimal UTS of > 300 MPa [73]. Tensile strength is dependent on the degree of crosslinking within the material. In such matter, elongation comes with a tradeoff in the reduction of UTS and YM, and therefore, a balance is typically necessary.

The longitudinal integrity of the stent can be of great importance due to the recent clinical observations that showed significant longitudinal compression or 'stent shortening' in several contemporary stents, which occurs during the re-crossing with other devices such as stent delivery systems, post-dilatation balloons, or catheters [57]. A clinically relevant longitudinal compression force was estimated, to which a stent could possibly be subjected in a case when a catheter tip is caught while crossing a stent. Although the LT 50 µm group appears to outperform the remainder configurations, no statistically significant difference was found between the groups. Also, all configurations showed only a small percentage of distortion, especially when comparing the results of the non-biodegradable stents (average 2,34%) to the 'Xience' (Abbot, USA) and the 'Promus Element' (Boston Scientific, USA), which are the two most commonly used stents worldwide [61]. These commercially available stents showed much greater displacement factors (3.57% and 17.86%, respectively). These results highlight that the longitudinal compression of different stents indicates that a deployed stent's tendency to undergo longitudinal compression is strongly associated with the design and the essential role of connectors. All non-biodegradable stents (4 connectors) showed significantly lower compression rates than the Xience (3 connectors) and the Promus Element (2 connectors). The hoops of the stent provide support, while the connectors hold the hoops together and thus prevent longitudinal distortion. However, increasing the number of connectors lowers the flexibility of the stent, which is unfavourable for the delivery process.

4.3. Morphological analysis

The morphological analysis was divided into three parts, investigating the influence of the printing layer thicknesses. First, a surface analysis was performed, which indicates that surface smoothness increases with the decrease in layer thickness. Samples comprising a layer thickness of 25 and 50 µm showed notably smoother surface finish than the 100 and 160 µm prints, which is endorsed by Schaub et al. [74], who identified that the lesser the thickness of the built layer, the finer is the surface finish. This previously mentioned difference primarily results from the curved 'step-layer' morphology. The lower layer thickness stents contained a relatively smooth surface, where an increase in layer thickness strongly accentuated a 'step-layer' interface. The latter is caused by the layer by layer fabrication, which will irrespectively be present unless really fine slicing of 1 µm or less is selected, curves will always arise. Apart from the step-layer surface, the overall surface finish between the configurations was reasonably similar. The latter is endorsed by the Interferometry results, suggesting no significant difference between the various configurations. Also, -as previously mentioned- several commercial companies endorsed this finding indicating that printing models at lower resolutions (i.e. thicker layer heights) can result in higher-quality prints. Yet, it is important to note that the Interferometry, as well as the AFM results, were obtained from a flat surface contrary to the round structure of the stent. Understandably, the shape of the sample can have a great influence on its surface finish and thus, it is hard to declare if the flat surface results are in a similar range as the round stent framework (Appendix G). Furthermore, the AFM was used to verify if the Interferometry results were accurate, showing somewhat similar results. It has to be emphasized that the Interferometry samples were 60 seconds gold-sputtered, increasing the surface with approximately an additional 5-10 nm. Furthermore, as mentioned in section 4.1, fabrication with SLA requires added support for printing spread structures and sufficient adhesion to the printing bed. The support material remains were observed at the attachment's areas (Appendix F) and are inherently connected to the selected fabrication method. So, initiation of support structures in a region that is not in contact with tissue will enhance a smoother surface finish. All the above-argued results insinuate that a smooth surface is crucial for the attachment of the stent to the tunica intima, which indeed is of great importance. By all means, surface topography is a critical determinant of the stent performance to reduce thrombogenicity and neointimal proliferation [75]; however, it is now suggested that rough surfaces may

accelerate stent endothelialization, a process that is believed to have a significant influence on reduced clot formation and neointimal growth after stent implantation. Simultaneously, the biotech industry improves the flat surfaces of the various metal stents to only several nanometers whilst manipulating the surface with a mixture of nanometer and submicron features to decrease platelet adhesion and enhance endothelial cell functions as well [76]. From a realistic point of view, it is obvious that such smooth surfaces are unattainable for additive manufacturing techniques at present. Nonetheless, Dibra et al. [77] finely showed the difference between equivalent rough-surface stents and smooth-surface stents concerning late lumen loss and restenosis. The 'rough' stent contained a minimum and maximum root mean square roughness value of 0.09 and 0.21 m, which is larger than the values of the non-biodegradable stents fabricated for the needs of this thesis (0.06 and 0.12 m). The research showed equivalent values between the two types of stent regarding late lumen loss and an interesting trend towards a reduced angiographic restenosis rate involving the 'rough' stent. Both types of stents were associated with similar rates of thrombosis-related events. Conclusively, surface topography remains a critical determinant for the stent performance; however, research endorsed no substantial difference between a 'smooth' and 'rough' surface stent, whilst the 'rough' stent brings the potential benefit of an increased drug-storing capacity.

Secondly, intersection structures of the prints were analyzed by initiating a crack in both the transverse plane and sagittal plane. Similar to the surface finish, LT 25 µm stents showed the most homogeneous structure, with over LT 50 and 100 µm prints. Although LT 25 µm samples were considered decent compared to the CoCr-stent, there still was a notable difference in both surface finish and intersection structure. However, it is important to note that there was a difference in the 'break' process of the different stents. The non-biodegradable stents were compressed to 75% of their original diameter, where the CoCr-stent was still intact after similar compression. Thus, the CoCr-stent was cut, which potentially could have a slight effect on its cross-sectional morphology. A homogeneous structure of implants results in an increased surface exposure to water, and thus a dissimilar and faster degradation process [69]. Studies [69][78] have defined four key degradation mechanism (for polymers): oxidation (due to oxidant produced by tissues), hydrolysis (reaction with water) and physical degradation (loading, mechanical stresses, and wear). The timeline in which one of these processes occur will differ and depend on polymer composition, polymer structure, molecular weight, impurities (e.g. catalysts), hydrophobicity and solvent residues. In addition, due to stresses, implants can form micro-cracks, resulting in increased surface exposure to water and thus a faster degradation process, but also biological factors such as blood flow and pH can influence the degradation process. Therefore, a homogeneous internal structure is essential.

Thirdly, the printing accuracy of the non-biodegradable stents was evaluated by measuring the strut thickness at eight specific points and evaluating the diameter among multiple prints. It is important to note that the CAD-file models were designed with an outer diameter of 3 mm, a strut thickness of 200 µm and a strut width of 195 µm. The latter is not analyzed due to the inevitable imprecision generated when imaging a round structure. Consequently, to minimize the angle influence, the stent length (CAD file) was attuned from 10 mm to 3 mm, and imaging occurred from above (proximal side). This study proved successful in printing high accurate prints up to 3 mm in outer diameter. However, inhomogeneous properties in strut thickness were observed in all non-biodegradable stents, with the slightest deviations in the LT 25 µm stents ascending to LT 50 µm and LT 100 µm stents. Nevertheless, market available strut thickness of about 150 to 200 µm, and an outer diameter of 3 mm was met for all stents.

4.4. Biodegradable alternative

Clinicians agreed that a permanent stent presents long-term disadvantages beyond the short-term benefits, arterial remodelling, drug release, and mechanical support [10][11]. Besides, restenosis is rarely seen later than 12 months after surgery, and so, the clinical need for stent scaffolding is likely to be very limited [40]. In addition, arterial patency is commonly recovered within the first six months after the procedure, which corresponds with the period for the potential start of in-stent restenosis [12]. All the arguments mentioned above endorse the statement that the use of a permanent stent is unfavourable. To overcome all the disadvantages and limitations of BMS and metallic DES, bioresorbable stents (BRS) have been developed. These devices offer short-term mechanical support to the vessel, after which they will dissolve and thus decrease chronic inflammation and improve vascular healing. BRS can be divided into metal stents and polymer-based stents.

By reason of the high sensitivity of SLA printing, the non-biodegradable (commercial) resin will disclose SLA restraints as a fabrication method for cardiovascular stents, while the biodegradable composition of van Lith et al. [39] is mimicked to ensure successful printing. The protocol of Lith et al.[39][54] was followed precisely; only the purification steps deviate as the option of freeze-drying was not available. Instead, an alternative purification method was deployed, using ethyl acetate. It is suggested that this chemical is (in) directly responsible for the high rate of viscosity of the resin by reason of a too early formed (network) polymer due to the high temperatures that are required to remove the ethyl acetate. A too viscous resin can hinder the polymerization process, or for that case, having a convex surface affecting printing quality. The addition of solvents reduces the viscosity of the resin, making it more practical. However, a too viscous resin may also affect the exposure strength required for curing [79]. The resin viscosity should be within the margin range of 35-4000 mPa·s for all SLA printable resin-viscosity's [59]. As viscosity proved to be an essential parameter, this research investigated the defined resins on this subject. The non-biodegradable resin viscosity was within the above-mentioned margin (1628 mPa·s); however, the biodegradable variant resin showed too high values (2.72 x 10x4 mPa·s). Another factor that could affect the synthesis itself, since temperature management was experienced as complicated. The latter is an important aspect since accurately regulated temperature is crucial for the synthesis. Consequently, an alternative could be the use of oil, as the temperature is more straightforward to manage.

This study endorsed that the current state of SLA additive manufacturing method is very promising but still not ideal for the printing of BRS. Several aspects such as radial strength, surface roughness, accuracy and limited material availability hamper the clinical implementation of this promising technology. The latter is essential for future development and is connected to all other properties. It is important to note that all characteristics are interconnected, and thus it is a trade-off seeking the correct balance between all those factors. Still, it was evident that currently, stereolithography printing provides the most acceptable option for printing small dimensions comprising a smooth surface. However, future research on suitable biomaterials, biodegradability and delivery is necessary for the advancement of SLA regarding BRS fabrication.

5

Conclusion

Although BRS potentially has long term benefits for resuming native coronary vasomotion, scientific proof is not yet available. Since the first BRS, Absorb GT1 (Abbott, USA) was FDA approved, a new shift was expected towards bioresorbable scaffolds. However, structural and mechanical limitations on current BRS are hampering the path to become a mainstream technology. The future of stent development is also linked to patient specific designs. The application of AM technology can facilitate fast on-the-spot and on-demand printing of patient-specific bioresorbable stents. As AM process, stereolithography will provide the most suitable method, as it comprises several essential features such as, high accuracy printing and smooth surface finish. Still, the biggest drawback is the limited biomaterials available for such methods.

This study aimed to contribute to innovations leading to the development of a next generation stent. It presents novel information on SLA usability for the 3D printing of BRS and the effect of printing layer thickness on the stents' properties, but also highlights the effects of -above mentioned- limitations, which are all inherent to the materials selection. Development and progress on specific capabilities has revealed and emphasized shortcomings in other domains. Fine-tuning the SLA printer settings and limitation, it was able to 3D print a non-biodegradable variant, involving a 3 mm stent with adequate mechanical and morphological characteristics. A support material angle of 40 degrees with respect to the printing bed, and a maximum of 4 samples per print, resulted in the highest print success rate. Nonetheless, the biodegradable alternative was not suitable for the SLA printing process, due to several errors in the synthesis of the B-ink resin.

The study on the mechanical properties of the non-biodegradable stents showed sufficient radial strength compared to the existing standards. The study indicates that radial strength increases with protracted post-processing times, only until 45 min. Most configurations exceeded the minimal standards, providing room for reduction concerning strut width and thickness. The effect of layer thickness on radial strength was remarkable since the LT 50 µm group exceeded the LT 25 µm and LT 100 µm stents. However, increasing the number of cycles to expose potential fatigue characteristics on the different configurations of all groups except for the LT 25 µm failed after 4200 cycles. Concerning the YM and UTS, all groups showed reasonable results compared to the minimal standards; however, improvements are crucial for further development. Remarkably, the longitudinal compression results indicated that all non-biodegradable groups outperformed the currently most-used-stents worldwide.

The morphological characteristics of the non-biodegradable stents were tolerable but not sufficient. A too-large difference was observed between the clinically used CoCr-stent and the 3D printed stents regarding surface finish and cross-sectional morphology. Nevertheless, this research disclosed that morphological properties decrease with the increase in layer thickness. The LT 25 µm configurations, which was the smallest layer thickness resolution applicable, showed the most promising result endorsing the previously mentioned argument. Subsequently, a smaller layer thickness resolution will enhance a smoother surface finish and more dense and homogeneous properties; however, it will also significantly increase fabrication time.

This research has shown that a narrowly focused approach has not led to a major breakthrough, and creative thinking regarding material selection as well as manufacturing methods are required to contribute to

innovations leading to the development of a next-generation stent. Future research and development should encompass all the aspects of stent application, from manufacturing to deliverability, from functionality to solvability.

6

Recommendations

Several aspects are crucial for further development of additively manufactured drug-eluting bioresorbable polymeric cardiovascular stents. Firstly, the deliverability of the scaffold or stent systems, which refers to the introduction and transportation through a bodily lumen into the desired vessel, is characterized by trackability, flexibility, and pushability [56]. To enhance trackability of the non-visible bioresorbable scaffold during intervention as well as the healing period, radiopaque markers are embedded to enable fluoroscopic visualization. The author suggests grafting holes at the proximal outer shafts where the (Platinum) markers will be incorporated after the printing process. Moreover, the correct deployment of the stent, which refers to the expansion within the lumen at the treatment region, is fundamental. In essence, polymers contain a larger crossing profile and offer limited crimping compared to metals [20]. Also, until now, the three-dimensional printed stents are post cured after printing, increasing their strength but reducing their flexibility. Subsequently, delivery and deployment for polymer BRS are impeded. To potentially solve the -above mentioned- issue, the delivery process can be inverted, so instead of crimping the scaffold on a balloon, crimping a balloon around a scaffold and then removing the balloon (or other alternative casing) enabling the balloon into its original state. It is important to note that all the above presented options are not based on existing literature but speculations of the author.

Secondly, incorporating drugs on/ or into the polymer matrix is essential to prevent in-stent-restenosis (IRS) and thus achieve better clinical outcomes. The ideal (drug-eluting) stent should comprise two roles to guarantee the protection of healthy endothelial function and growth. On the one hand, it should adequately inhibit vascular smooth muscle cell proliferation. On the other hand, it should destruct fewer endothelial cells. Clinical evidence supports the superiority of Sirolimus-eluting stents over Paclitaxel eluting stents regarding safety, and anti-restenosis efficiency [80]. Thus, it is the primary anti-proliferative agent utilized in coronary DES. A controlled drug release in the arterial wall for 30-90 days is crucial for attaining inhibition of neointimal formation. Generally, stents are developed using a surface coating of either polymeric or metallic scaffolding, containing a polymeric carrier that includes a (bio)active agent or anti-proliferative drug. Conversely, another option is to incorporate the drug into the polymer matrix. Since SLA is being deployed as a manufacturing method, a benefit is that drugs can be mixed with the photopolymer prior to printing and become trapped in the solidified matrices [81]. However, the suitability of the correct drug, with modified release characteristics, should be evaluated. This is because the laser beam used to photopolymerize monomers must not influence the drug's effectiveness. Yet, to the best of the authors' knowledge, there have been only a few attempts to explore SLA three-dimensional printing's potential to manufacture modified drug released scaffolds. An important feature is that the polymer-based coating/ drugs should also facilitate biocompatibility, it cannot interact with active drugs, and it should share a platform for suitable drug-eluting kinetics. Also, it must act biologically inert once the drug has fully been eluted, and it must be mechanically stable [82]. Moreover, an additional important aspect is that the selected drugs must be thermally labile. The ICH guideline S10 on photosafety of pharmaceuticals is established between 360 and 400 nm. Further research on suitable active pharmaceutical ingredients (API) is required to set the stage for drug incorporation development leading to novel innovations, which can be applied in the next generation of stents.

Thirdly, the correct degradation time is essential for a safe and successful clinical treatment. There are two

different time frames regarding bioresorbable scaffolds. Functional time means the duration of a degradable polymer in which it maintains its desired function under applied conditions. Disappearance time means the time a polymer takes to fully degrade and lose mass. Between those two times, resorbable materials lose their mechanical reliability and thus release their degradation products. The latter can be concerning as these can cause undesirable physiological responses [83]. Degradation of resorbable polymers is linked to various polymer properties and is generally observed by tracing the biomaterials' mass loss, material function and molar mass change. Furthermore, as the strength of the material decreases, the chances of a collapse of the scaffold increases. Besides, the deepened knowledge of how the biomaterial exactly degrades, meaning which chemicals are released during degradation and are these cytotoxic or not, is crucial to know and to understand. So, it is crucial to characterize the degradation cycle in detail to prevent severe complications.

Bibliography

[1] Robert Beaglehole, Rodolfo Saracci, and Salvatore Panico. Cardiovascular diseases: causes, surveillance and prevention. *International Journal of Epidemiology*, 30(suppl_1):S1, 2001.

[2] World Health Organization et al. *Global status report on noncommunicable diseases 2014*. Number WHO/NMH/NVI/15.1. World Health Organization, 2014.

[3] Guido Stoll and Martin Bendszus. Inflammation and atherosclerosis: novel insights into plaque formation and destabilization. *Stroke*, 37(7):1923–1932, 2006.

[4] Herbert C Stary, A Bleakley Chandler, Robert E Dinsmore, Valentin Fuster, Seymour Glagov, William Insull Jr, Michael E Rosenfeld, Colin J Schwartz, William D Wagner, and Robert W Wissler. A definition of advanced types of atherosclerotic lesions and a histological classification of atherosclerosis: a report from the committee on vascular lesions of the council on arteriosclerosis, american heart association. *Circulation*, 92(5):1355–1374, 1995.

[5] William Insull Jr. The pathology of atherosclerosis: plaque development and plaque responses to medical treatment. *The American journal of medicine*, 122(1):S3–S14, 2009.

[6] Jean-Michel Serfaty, Linda Chaabane, André Tabib, Jean-Michel Chevallier, André Briguet, and Phillippe C Douek. Atherosclerotic plaques: classification and characterization with t2-weighted high-spatial-resolution mr imaging—an in vitro study. *Radiology*, 219(2):403–410, 2001.

[7] Emilio B Lobato. Care of the patient with coronary stents undergoing noncardiac surgery. *Essentials of Cardiac Anesthesia for Noncardiac Surgery E-Book: A Companion to Kaplan's Cardiac Anesthesia*, page 32, 2018.

[8] Javaid Iqbal, Julian Gunn, and Patrick W Serruys. Coronary stents: historical development, current status and future directions. *British medical bulletin*, 106(1), 2013.

[9] Sahil Khera, Dhaval Kolte, and Deepak L Bhatt. Percutaneous coronary intervention. In *Translational Research in Coronary Artery Disease*, pages 179–194. Elsevier, 2016.

[10] John A Ormiston and Patrick WS Serruys. Bioabsorbable coronary stents. *Circulation: Cardiovascular Interventions*, 2(3):255–260, 2009.

[11] Niels Grabow, David P Martin, Klaus-Peter Schmitz, and Katrin Sternberg. Absorbable polymer stent technologies for vascular regeneration. *Journal of Chemical Technology & Biotechnology*, 85(6):744–751, 2010.

[12] Krassen Nedeltchev, Stefan Bickel, Marcel Arnold, Hakan Sarikaya, Dimitrios Georgiadis, Matthias Sturzenegger, Heinrich P Mattle, and Ralf W Baumgartner. Recanalization of spontaneous carotid artery dissection. *Stroke*, 40(2):499–504, 2009.

[13] Atul S Rao, Michel S Makaroun, Luke K Marone, Jae S Cho, Robert Rhee, and Rabih A Chaer. Long-term outcomes of internal carotid artery dissection. *Journal of vascular surgery*, 54(2):370–375, 2011.

[14] Kenya Brothers PhD Division of Cardiovascular Devices Office of Device Evaluation Food and Drug Administration. Absorb gt1 bioresorbable vascular scaffold (bvs) system, fda review of p150023. `https://www.fda.gov/media/96690/download`, March 2016. (Accessed on 11/30/2020).

[15] Bill D Gogas, James J Benham, Steve Hsu, Alexander Sheehy, David J Lefer, Traci T Goodchild, David J Polhemus, Yasir H Bouchi, Olivia Y Hung, Sang-Yong Yoo, et al. Vasomotor function comparative assessment at 1 and 2 years following implantation of the absorb everolimus-eluting bioresorbable vascular scaffold and the xience v everolimus-eluting metallic stent in porcine coronary arteries: insights from in vivo angiography, ex vivo assessment, and gene analysis at the stented/scaffolded segments and the proximal and distal edges. *JACC: Cardiovascular Interventions*, 9(7):728–741, 2016.

[16] Patrick W Serruys, Bernard Chevalier, Dariusz Dudek, Angel Cequier, Didier Carrié, Andres Iniguez, Marcello Dominici, René J van der Schaaf, Michael Haude, Luc Wasungu, et al. A bioresorbable everolimus-eluting scaffold versus a metallic everolimus-eluting stent for ischaemic heart disease caused by de-novo native coronary artery lesions (absorb ii): an interim 1-year analysis of clinical and procedural secondary outcomes from a randomised controlled trial. *The Lancet*, 385(9962):43–54, 2015.

[17] Bernard Chevalier, Maik Grundeken, Roseann White, Yuki Ishibashi, Hector Garcia Garcia, Yoshinobu Onuma, and Patrick Serruys. Differences in the occurrence of new or worsening angina between the absorb bioresorbable vascular scaffold and xience metallic stent: A post-hoc analysis of the absorb ii randomized trial. *Journal of the American College of Cardiology*, 65(10S):A1707–A1707, 2015.

[18] Charis Costopoulos, Azeem Latib, Toru Naganuma, Tadashi Miyazaki, Katsumasa Sato, Filippo Figini, Alessandro Sticchi, Mauro Carlino, Alaide Chieffo, Matteo Montorfano, et al. Comparison of early clinical outcomes between absorb bioresorbable vascular scaffold and everolimus-eluting stent implantation in a real-world population. *Catheterization and Cardiovascular Interventions*, 85(1):E10–E15, 2015.

[19] Alessio Mattesini, Gioel G Secco, Gianni Dall'Ara, Matteo Ghione, Juan C Rama-Merchan, Alessandro Lupi, Nicola Viceconte, Alistair C Lindsay, Ranil De Silva, Nicolas Foin, et al. Absorb biodegradable stents versus second-generation metal stents: a comparison study of 100 complex lesions treated under oct guidance. *JACC: Cardiovascular interventions*, 7(7):741–750, 2014.

[20] Ryan D Alexy and Daniel S Levi. Materials and manufacturing technologies available for production of a pediatric bioabsorbable stent. *BioMed research international*, 2013, 2013.

[21] John A Bittl. Bioresorbable stents: the next revolution, 2010.

[22] Lei Yang, Xin Chen, Lei Zhang, Lei Li, Shuangzhu Kang, Chengjin Wang, and Wei Sun. Additive manufacturing in vascular stent fabrication. In *MATEC Web of Conferences*, volume 253, page 03003. EDP Sciences, 2019.

[23] Sandra Pina, Viviana P Ribeiro, Catarina F Marques, F Raquel Maia, Tiago H Silva, Rui L Reis, and J Miguel Oliveira. Scaffolding strategies for tissue engineering and regenerative medicine applications. *Materials*, 12(11):1824, 2019.

[24] Tiziana Fuoco, Astrid Ahlinder, Shubham Jain, Kamal Mustafa, and Anna Finne-Wistrand. Poly (ε-caprolactone-co-p-dioxanone): a degradable and printable copolymer for pliable 3d scaffolds fabrication toward adipose tissue regeneration. *Biomacromolecules*, 21(1):188–198, 2019.

[25] Ishita Matai, Gurvinder Kaur, Amir Seyedsalehi, Aneesah McClinton, and Cato T Laurencin. Progress in 3d bioprinting technology for tissue/organ regenerative engineering. *Biomaterials*, 226:119536, 2020.

[26] Allison M Pekkanen, Ryan J Mondschein, Christopher B Williams, and Timothy E Long. 3d printing polymers with supramolecular functionality for biological applications. *Biomacromolecules*, 18(9):2669–2687, 2017.

[27] Ryan J Mondschein, Akanksha Kanitkar, Christopher B Williams, Scott S Verbridge, and Timothy E Long. Polymer structure-property requirements for stereolithographic 3d printing of soft tissue engineering scaffolds. *Biomaterials*, 140:170–188, 2017.

[28] J Fajardo Cortes. 3d printing of patient specific bioresorbable cardiovascular stents. `file:///Users/thomasvandenbrekel/Downloads/Thesis_Report_.pdf`, August 2017. (Accessed on 11/30/2020).

[29] Alvaro Goyanes, Usanee Det-Amornrat, Jie Wang, Abdul W Basit, and Simon Gaisford. 3d scanning and 3d printing as innovative technologies for fabricating personalized topical drug delivery systems. *Journal of controlled release*, 234:41–48, 2016.

[30] Gabriele Taormina, Corrado Sciancalepore, Massimo Messori, and Federica Bondioli. 3d printing processes for photocurable polymeric materials: technologies, materials, and future trends. *Journal of applied biomaterials & functional materials*, 16(3):151–160, 2018.

[31] Ian Gibson Ian Gibson. Additive manufacturing technologies 3d printing, rapid prototyping, and direct digital manufacturing, 2015.

[32] CS Lim, P Eng, SC Lin, CK Chua, and YT Lee. Rapid prototyping and tooling of custom-made tracheobronchial stents. *The International Journal of Advanced Manufacturing Technology*, 20(1):44–49, 2002.

[33] Mohammad Vaezi, Hermann Seitz, and Shoufeng Yang. A review on 3d micro-additive manufacturing technologies. *The International Journal of Advanced Manufacturing Technology*, 67(5-8):1721–1754, 2013.

[34] John R Tumbleston, David Shirvanyants, Nikita Ermoshkin, Rima Janusziewicz, Ashley R Johnson, David Kelly, Kai Chen, Robert Pinschmidt, Jason P Rolland, Alexander Ermoshkin, et al. Continuous liquid interface production of 3d objects. *Science*, 347(6228):1349–1352, 2015.

[35] Henry Oliver T Ware, Adam C Farsheed, Robert Van Lith, Evan Baker, Guillermo Ameer, and Cheng Sun. Process development for high-resolution 3d-printing of bioresorbable vascular stents. In *Advanced Fabrication Technologies for Micro/Nano Optics and Photonics X*, volume 10115, page 101150N. International Society for Optics and Photonics, 2017.

[36] Sla - stereolithography (and dlp, cdlp, clip). `https://www.additive.blog/knowledge-base/3d-printers/sla-stereolithography-dlp-cdlp-clip/`. (Accessed on 11/30/2020).

[37] KD Triantafyllou, S Frangoulis, and TM Kolettis. Coronary endarterectomy and stent removal with off-pump coronary artery bypass surgery. *Heart*, 92(7):885–885, 2006.

[38] Nicolas Foin, Renick D Lee, Ryo Torii, Juan Luis Guitierrez-Chico, Alessio Mattesini, Sukhjinder Nijjer, Sayan Sen, Ricardo Petraco, Justin E Davies, Carlo Di Mario, et al. Impact of stent strut design in metallic stents and biodegradable scaffolds. *International journal of cardiology*, 177(3):800–808, 2014.

[39] Robert Van Lith, Evan Baker, Henry Ware, Jian Yang, Adam Cyrus Farsheed, Cheng Sun, and Guillermo Ameer. 3d-printing strong high-resolution antioxidant bioresorbable vascular stents. *Advanced Materials Technologies*, 1(9):1600138, 2016.

[40] Joel A Kaplan. *Essentials of Cardiac Anesthesia for Noncardiac Surgery E-Book: A Companion to Kaplan's Cardiac Anesthesia*. Elsevier Health Sciences, 2018.

[41] Bill D Gogas. Bioresorbable scaffolds for percutaneous coronary interventions. *Global Cardiology Science and Practice*, 2014(4):55, 2015.

[42] Michael Arthur Cuiffo, Jeffrey Snyder, Alicia M Elliott, Nicholas Romero, Sandhiya Kannan, and Gary P Halada. Impact of the fused deposition (fdm) printing process on polylactic acid (pla) chemistry and structure. *Applied Sciences*, 7(6):579, 2017.

[43] Leevameng Bouapao, Hideto Tsuji, Kohji Tashiro, Jianming Zhang, and Makoto Hanesaka. Crystallization, spherulite growth, and structure of blends of crystalline and amorphous poly (lactide) s. *Polymer*, 50(16):4007–4017, 2009.

[44] John Canfield and Hana Totary-Jain. 40 years of percutaneous coronary intervention: history and future directions. *Journal of personalized medicine*, 8(4):33, 2018.

[45] Yosinobu Onuma and Patrick W Serruys. Bioresorbable scaffold: the advent of a new era in percutaneous coronary and peripheral revascularization? *Circulation*, 123(7):779–797, 2011.

[46] Maria Ann Woodruff and Dietmar Werner Hutmacher. The return of a forgotten polymer—polycaprolactone in the 21st century. *Progress in polymer science*, 35(10):1217–1256, 2010.

[47] J Fernández, E Meaurio, A Chaos, A Etxeberria, A Alonso-Varona, and JR Sarasua. Synthesis and characterization of poly (l-lactide/ε-caprolactone) statistical copolymers with well resolved chain microstructures. *Polymer*, 54(11):2621–2631, 2013.

[48] Scott A Guelcher, Katie M Gallagher, Jonathan E Didier, Derek B Klinedinst, John S Doctor, Aaron S Goldstein, Garth L Wilkes, Eric J Beckman, and Jeffrey O Hollinger. Synthesis of biocompatible segmented polyurethanes from aliphatic diisocyanates and diurea diol chain extenders. *Acta Biomaterialia*, 1(4):471–484, 2005.

[49] Monika Bil, Joanna Ryszkowska, Piotr Woźniak, Krzysztof J Kurzydłowski, and Małgorzata Lewandowska-Szumieł. Optimization of the structure of polyurethanes for bone tissue engineering applications. *Acta biomaterialia*, 6(7):2501–2510, 2010.

[50] Breno Rocha Barrioni, Sandhra Maria de Carvalho, Rodrigo Lambert Oréfice, Agda Aline Rocha de Oliveira, and Marivalda de Magalhães Pereira. Synthesis and characterization of biodegradable polyurethane films based on hdi with hydrolyzable crosslinked bonds and a homogeneous structure for biomedical applications. *Materials Science and Engineering: C*, 52:22–30, 2015.

[51] James V Crivello and Elsa Reichmanis. Photopolymer materials and processes for advanced technologies. *Chemistry of Materials*, 26(1):533–548, 2014.

[52] Samuel Clark Ligon-Auer, Martin Schwentenwein, Christian Gorsche, Jürgen Stampfl, and Robert Liska. Toughening of photo-curable polymer networks: a review. *Polymer Chemistry*, 7(2):257–286, 2016.

[53] Sean S Moore, Kevin J O'Sullivan, and Francesco Verdecchia. Shrinking the supply chain for implantable coronary stent devices. *Annals of biomedical engineering*, 44(2):497–507, 2016.

[54] Jian Yang, Antonio R Webb, and Guillermo A Ameer. Novel citric acid-based biodegradable elastomers for tissue engineering. *Advanced Materials*, 16(6):511–516, 2004.

[55] Formlabs. Materials library.pdf. `file:///Users/thomasvandenbrekel/Downloads/Materials%20Library.pdf`, 7 2019. (Accessed on 12/07/2020).

[56] Wolfram Schmidt, Peter Behrens, Christoph Brandt-Wunderlich, Stefan Siewert, Niels Grabow, and Klaus-Peter Schmitz. In vitro performance investigation of bioresorbable scaffolds–standard tests for vascular stents and beyond. *Cardiovascular Revascularization Medicine*, 17(6):375–383, 2016.

[57] Santosh Prabhu, Tanya Schikorr, Tamer Mahmoud, James Jacobs, Adriaan Potgieter, and Charles Simonton. Engineering assessment of the longitudinal compression behaviour of contemporary coronary stents. *EuroIntervention: journal of EuroPCR in collaboration with the Working Group on Interventional Cardiology of the European Society of Cardiology*, 8(2):275–281, 2012.

[58] Paul D Williams, Mamas A Mamas, Kenneth P Morgan, Magdi El-Omar, Bernard Clarke, Anthony Bainbridge, Farzin Fath-Ordoubadi, and Douglas G Fraser. Longitudinal stent deformation: a retrospective analysis of frequency and mechanisms. *EuroIntervention: journal of EuroPCR in collaboration with the Working Group on Interventional Cardiology of the European Society of Cardiology*, 8(2):267, 2012.

[59] H Does. Stereolithography 3d printing of bio-photopolymer resin. `file:///Users/thomasvandenbrekel/Downloads/Thesis_Henry_Does_13005952.pdf`, April 2020. (Accessed on 11/30/2020).

[60] IWL Gore et al. Mechanical properties of nitinol stents and stent-grafts: Comparison of 6mm diameter devices. 2007.

[61] K. (Ph.D) Zamanian. Cardiac stent usage among u.s. `https://www.dicardiology.com/article/cardiac-stent-usage-among-us-cardiologists`, 2012. (Accessed on 12/15/2020).

[62] Ferry PW Melchels, Jan Feijen, and Dirk W Grijpma. A review on stereolithography and its applications in biomedical engineering. *Biomaterials*, 31(24):6121–6130, 2010.

[63] Bethany C Gross, Jayda L Erkal, Sarah Y Lockwood, Chengpeng Chen, and Dana M Spence. Evaluation of 3d printing and its potential impact on biotechnology and the chemical sciences, 2014.

[64] Andrew A Gill and Frederik Claeyssens. 3d structuring of biocompatible and biodegradable polymers via stereolithography. pages 309–321, 2011.

[65] Afsoon Farzan, Sedigheh Borandeh, Nazanin Zanjanizadeh Ezazi, Sami Lipponen, Hélder A Santos, and Jukka Seppälä. 3d scaffolding of fast photocurable polyurethane for soft tissue engineering by stereolithography: Influence of materials and geometry on growth of fibroblast cells. *European Polymer Journal*, 139:109988, 2020.

[66] Kent R Miller and Mark D Soucek. Photopolymerization of biocompatible films containing poly (lactic acid). *European Polymer Journal*, 48(12):2107–2116, 2012.

[67] K Chockalingam, N Jawahar, and U Chandrasekhar. Influence of layer thickness on mechanical properties in stereolithography. *Rapid Prototyping Journal*, 2006.

[68] QF Polosky, R Malloy, and R Stacer. A mechanical property performance comparison for plastic parts produced in a rapid epoxy tool and conventional steel tooling. 3:2972–2976, 1998.

[69] C Mauli Agrawal and Robert B Ray. Biodegradable polymeric scaffolds for musculoskeletal tissue engineering. *Journal of Biomedical Materials Research: An Official Journal of The Society for Biomaterials, The Japanese Society for Biomaterials, and The Australian Society for Biomaterials and the Korean Society for Biomaterials*, 55(2):141–150, 2001.

[70] Suresh Jayanthi, Bronson Hokuf, and John Lawton. Influence of post curing conditions on the mechanical properties of stereolithographic photopolymers. In *1995 International Solid Freeform Fabrication Symposium*, 1995.

[71] Asais Camila Uzcategui, Archish Muralidharan, Virginia L Ferguson, Stephanie J Bryant, and Robert R McLeod. Understanding and improving mechanical properties in 3d printed parts using a dual-cure acrylate-based resin for stereolithography. *Advanced engineering materials*, 20(12):1800876, 2018.

[72] Center for Devices and Radiological Health. Non-clinical engineering tests and recommended labeling for intravascular stents and associated delivery systems - guidance for industry and fda staff | fda. `https://www.fda.gov/regulatory-information/search-fda-guidance-documents/non-clinical-engineering-tests-and-recommended-labeling-intravascular-stents-and-associated-delive` April 2010. (Accessed on 05/10/2021).

[73] Irsalan Cockerill, Carmine Wang See, Marcus L Young, Yadong Wang, and Donghui Zhu. Designing better cardiovascular stent materials: A learning curve. *Advanced Functional Materials*, 31(1):2005361, 2021.

[74] Diane A Schaub and Douglas C Montgomery. Using experimental design to optimize the stereolithography process. *Quality Engineering*, 9(4):575–585, 1997.

[75] I De Scheerder, Eric Verbeken, and Jan Van Humbeeck. Metallic surface modification. In *Seminars in interventional cardiology: SIIC*, volume 3, pages 139–144, 1998.

[76] Jing Lu, Chang Yao, Lei Yang, and Thomas J Webster. Decreased platelet adhesion and enhanced endothelial cell functions on nano and submicron-rough titanium stents. *Tissue Engineering Part A*, 18 (13-14):1389–1398, 2012.

[77] Alban Dibra, Adnan Kastrati, Julinda Mehilli, Jürgen Pache, Randolf von Oepen, Josef Dirschinger, and Albert Schömig. Influence of stent surface topography on the outcomes of patients undergoing coronary stenting: A randomized double-blind controlled trial. *Catheterization and cardiovascular interventions*, 65(3):374–380, 2005.

[78] Magdy MM Elnashar et al. Immobilized molecules using biomaterials and nanobiotechnology. *Journal of Biomaterials and Nanobiotechnology*, 1(01):61, 2010.

[79] Malcolm N Cooke, John P Fisher, David Dean, Clare Rimnac, and Antonios G Mikos. Use of stereolithography to manufacture critical-sized 3d biodegradable scaffolds for bone ingrowth. *Journal of Biomedical Materials Research Part B: Applied Biomaterials: An Official Journal of The Society for Biomaterials, The Japanese Society for Biomaterials, and The Australian Society for Biomaterials and the Korean Society for Biomaterials*, 64(2):65–69, 2003.

[80] Adnan Kastrati, Alban Dibra, Sonja Eberle, Julinda Mehilli, José Suárez de Lezo, Jean-Jacque Goy, Kurt Ulm, and Albert Schömig. Sirolimus-eluting stents vs paclitaxel-eluting stents in patients with coronary artery disease: meta-analysis of randomized trials. *Jama*, 294(7):819–825, 2005.

[81] Jie Wang, Alvaro Goyanes, Simon Gaisford, and Abdul W Basit. Stereolithographic (sla) 3d printing of oral modified-release dosage forms. *International journal of pharmaceutics*, 503(1-2):207–212, 2016.

[82] Konstantinos D Rizas and Julinda Mehilli. Stent polymers: do they make a difference? *Circulation: Cardiovascular Interventions*, 9(6):e002943, 2016.

[83] Georgio Kfoury, Jean-Marie Raquez, Fatima Hassouna, Jérémy Odent, Valérie Toniazzo, David Ruch, and Philippe Dubois. Recent advances in high performance poly (lactide): from "green" plasticization to super-tough materials via (reactive) compounding. *Frontiers in Chemistry*, 1:32, 2013.

A

AM technique comparision

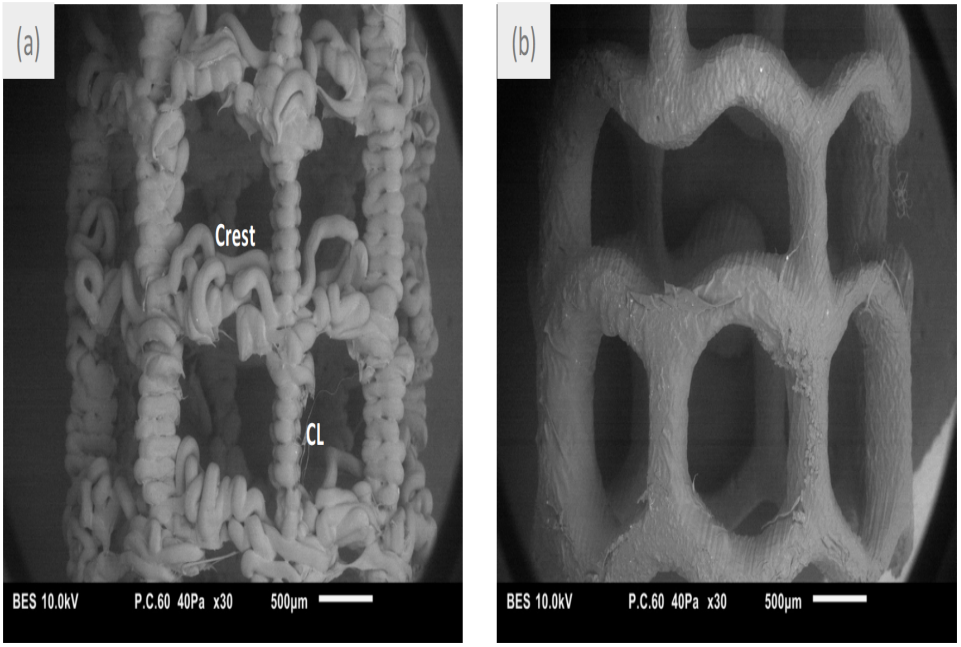

Figure 13 - SEM image comparison of a printed stent with the (a) Ultimaker 2+ and with the (b) Form 1+. Qualitative observation of the images shows the difference in accuracy and surface finish of both techniques. Moreover, (a) presents the layer-by-layer printing which is performed in the Z-direction, for both crests and connecting links (CL).

Figure A.1: Research by Cortes (2017) [28] compared various 3D printing techniques and endorsed the selection of SLA over FDM.

B

CAD-file

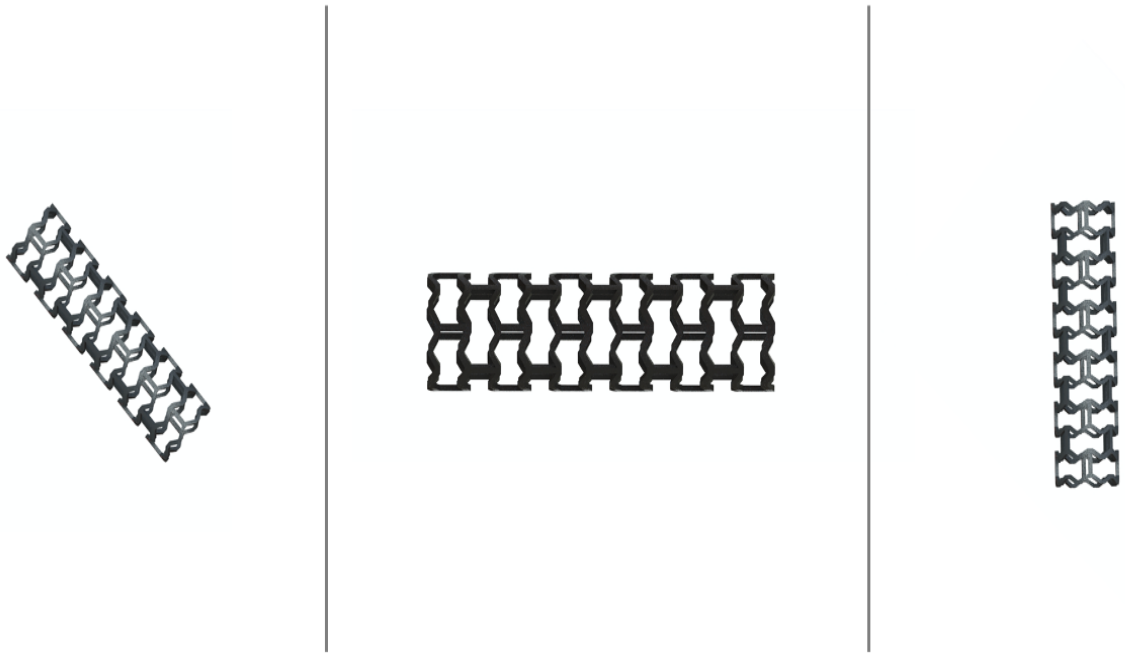

Figure B.1: The design was rendered with SolidWorks (Dassault Systèmes SolidWorks Corp., USA) (CAD files upon request).

C

SolidWorks simulation

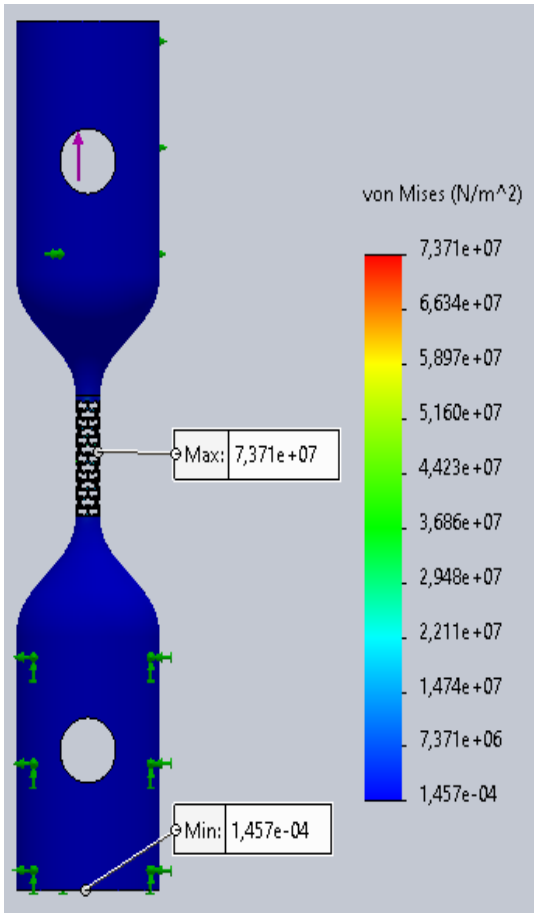

Figure C.1: A SolidWorks (Dassault Systèmes SolidWorks Corp., USA) simulation of uniaxial tensile testing to determine if the load distribution within the customized tensile bar was accurate.

D

Reference spectrum

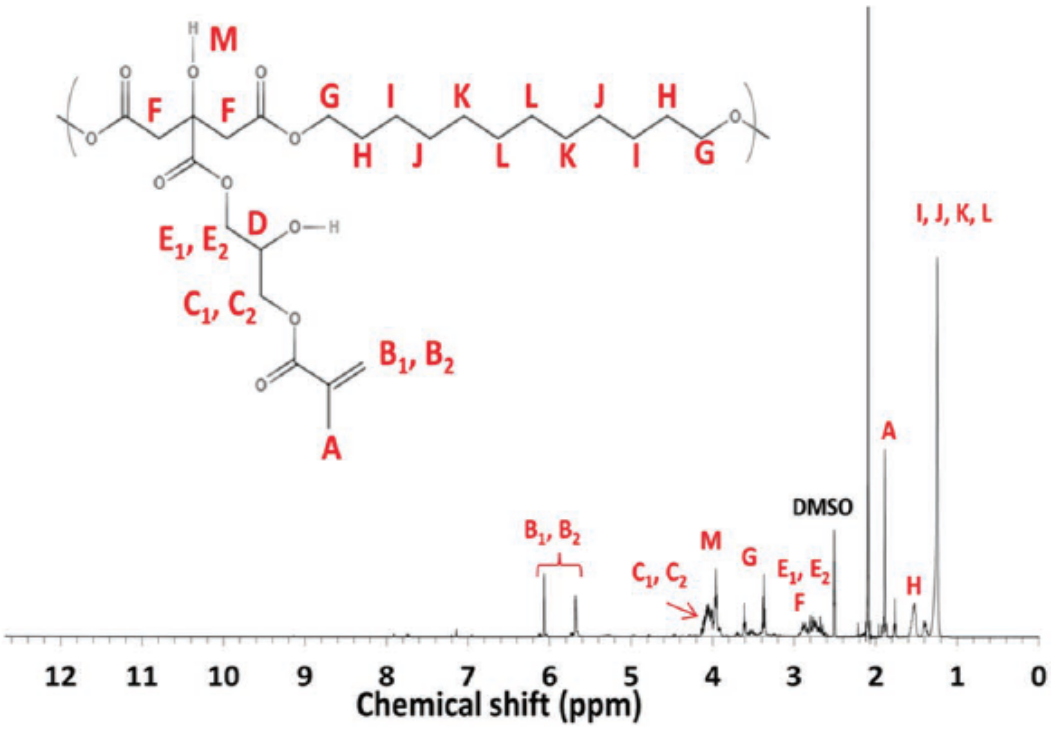

Figure D.1: Van Lith et al. [39] reference spectrum.

E

SEM images - section distribution

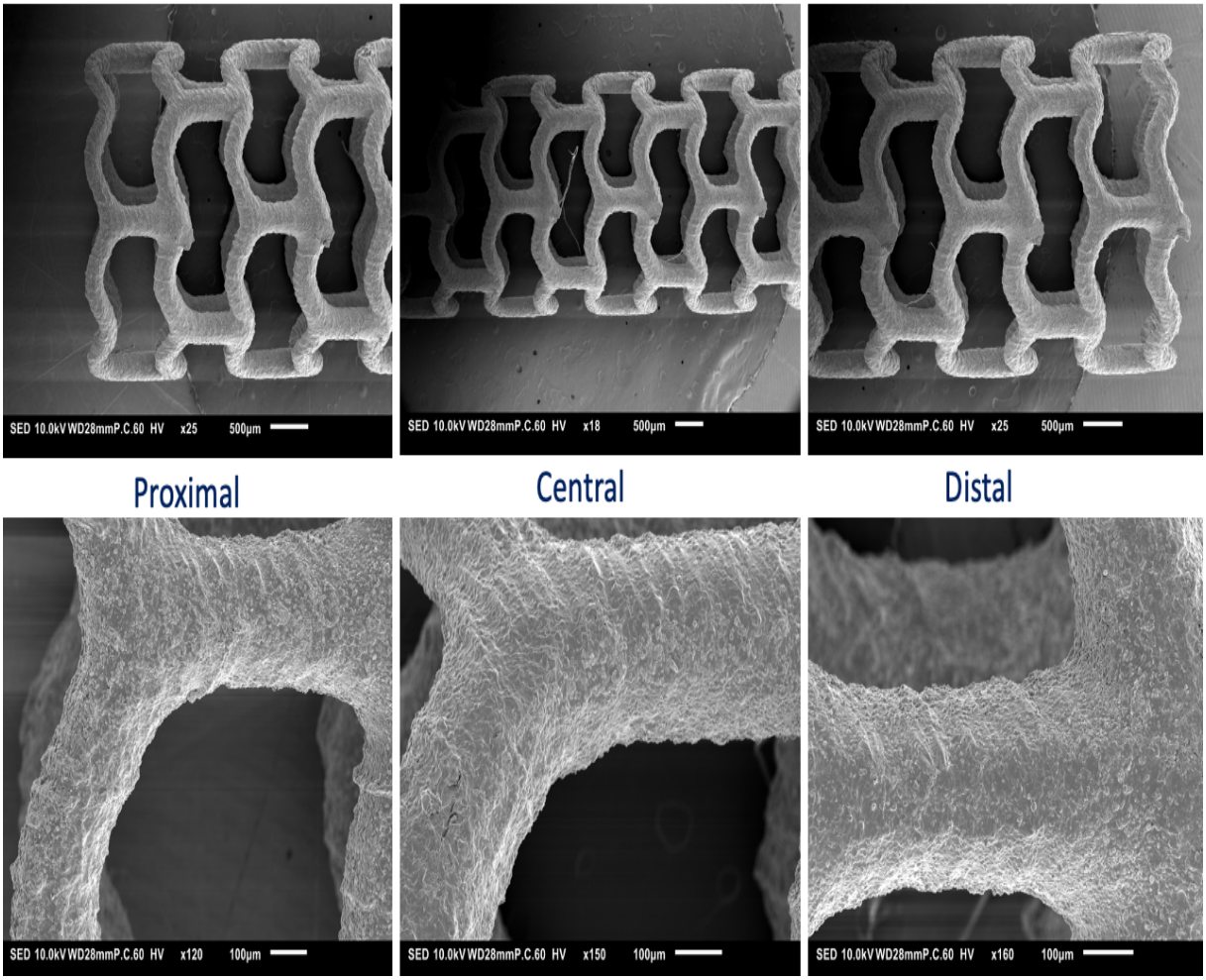

Figure E.1: The proximal, central and distal section of a non-biodegradable stent, OD 3 mm/ ST 200 µm/ LT 25 µm.

F

SEM images - support

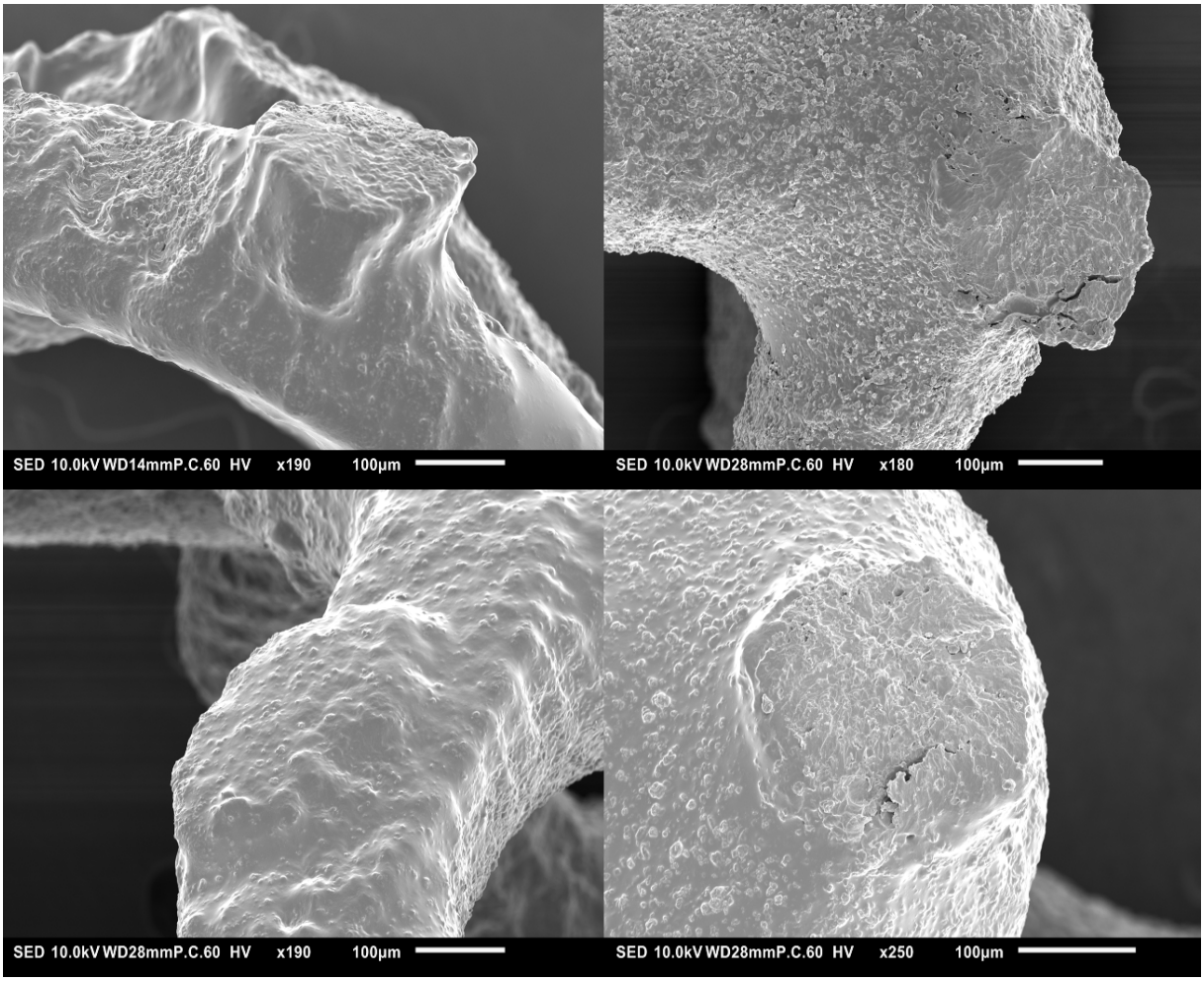

Figure F.1: The remains of the support material were observed at the attachment's areas

G

SEM images - flat samples

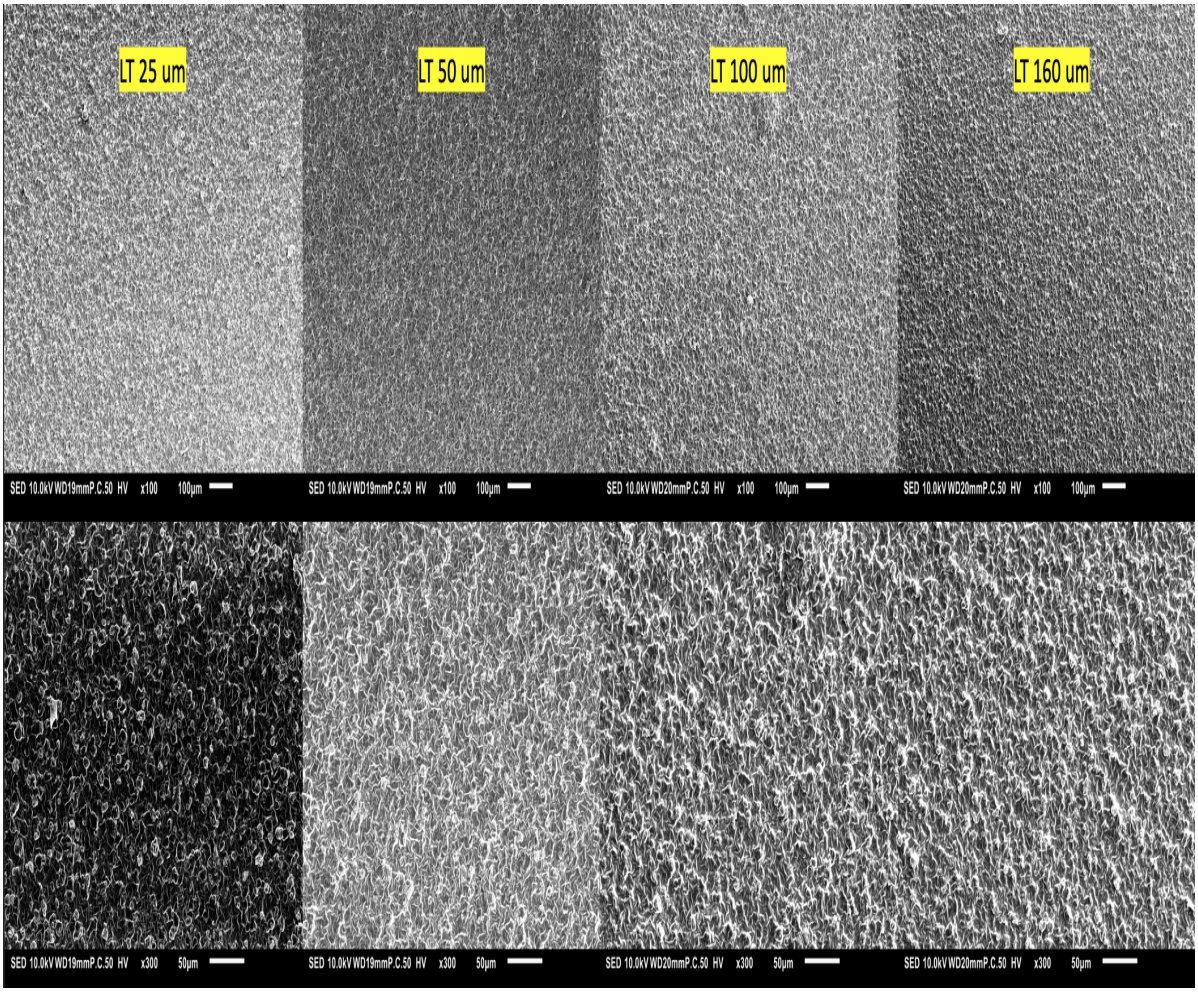

Figure G.1: SEM images of flat samples obtained from different layer thickness resolutions.